Improved predictions of contaminant transport in rivers

by

Rusen Sinir

A dissertation submitted to the graduate faculty

in partial fulfillment of the requirements for the degree of

DOCTOR OF PHILOSOPHY

Major: Civil Engineering (Environmental Engineering)

Program of Study Committee:
Chris Robert Rehmann, Co-major Professor
Halil Ceylan, Co-major Professor
Say Kee Ong
Roy Ruochuan Gu
Kristie Jean Franz

The student author, whose presentation of the scholarship herein was approved by the program of study committee, is solely responsible for the content of this dissertation. The Graduate College will ensure this dissertation is globally accessible and will not permit alterations after a degree is conferred.

Iowa State University

Ames, Iowa

2017

Copyright © Rusen Sinir, 2017. All rights reserved.

DEDICATION

This dissertation is dedicated to my wife Ismihan, my son, Kursat Cemil, my parents, Ahmet Gursat and Nazmiye, my sister, Sumeyye, and those who supported me throughout my education.

TABLE OF CONTENTS

Page

LIST OF FIGURES v

LIST OF TABLES vii

NOMENCLATURE viii

ACKNOWLEDGMENTS xiii

ABSTRACT xiv

CHAPTER 1. INTRODUCTION 1

Significance and Problem Definition 1

Objectives 4

Organization of the Dissertation 5

References 5

CHAPTER 2. FURTHER ANALYTICAL SOLUTIONS FOR CONTAMINANT TRANSPORT IN THE ADVECTIVE ZONE OF A RIVER 7

Abstract 7

Introduction 7

Methods 10

Results 13

Discussion 17

Conclusions 20

References 20

Appendix. Computation of Spatial and Temporal Moments 22

CHAPTER 3. ANALYTICAL SOLUTION OF TWO-STORAGE MODEL FOR INSTANTANEOUS SLUG RELEASE 25

Abstract 25

Introduction 25

Methods 29

Results and Discussion 34

Conclusions 38

References 39

Appendix. Computation of Temporal Moments 42

CHAPTER 4. PREDICTING TRACER RESPONSE CURVES WITH CONSTANT SKEWNESS 43

Abstract 43

Introduction 43

Methods 46

Evaluating the Jobson method 46

The proposed method 48

Results and Discussion 50

Skewness predicted by the Jobson method 50

Evaluation of the proposed method 51

Conclusions 58

References 59

CHAPTER 5. GENERAL CONCLUSIONS 61

Summary 61

Significant Findings 61

Future Work 62

LIST OF FIGURES

Page

Fig. 2.1. Evolution of parameters computed from spatial moments: (a) position of the centroid; (b) variance; (c) rate of change of the variance; (d) skewness. Results are computed for $\alpha = 0.15$. 13

Fig. 2.2. Comparison of the spatial moments for a spill in the stagnant zone and a spill in the flowing zone. 14

Fig. 2.3. Comparison of tracer-response curves for a spill in the stagnant zone (solid line) and a spill in the flowing zone (dotted line). The initial mass is the same. 15

Fig. 2.4. Comparison of R&W model and ADE for the case of a maintained injection in the flowing zone. Results are computed for $\alpha = 0.15$, $\beta = 4.5 \times 10^{-3}$ s^{-1}, and $U = 0.6$ m/s. 17

Fig. 3.1. (a) Effect of variable β_h by setting β_s constant for $\alpha_s = \alpha_h$ (b) effects of variable α_h by setting α_s constant for $\beta_h = \beta_s$ on the concentration curves with $\varepsilon = 0.0011$. 34

Fig. 3.2. Effects of variable α_h and β_h by setting α_s and β_s constant on (a) the arrival time of the centroid, (b) variance, (c) skewness coefficient, (d) kurtosis ($\varepsilon = 0.0011$ constant for all) 35

Fig. 3.3. Fitting current model to 2011 field experiment data from Johnson et al. (2014) 36

Fig. 3.4. Fitting current model to 2012 field experiment data from Johnson et al. (2014) 37

Fig. 4.1. Schematic of the peak concentration C_p and arrival times of the leading edge (t_L), peak concentration (t_P), and trailing edge (t_T). The leading and trailing edges are defined in terms of a fraction ϕ of the peak concentration. ... 50

Fig. 4.2. Decrease in the skewness coefficient computed for rivers with flows ranging from 10^{-1} m^3/s to 10^3 m^3/s. 51

Fig. 4.3. Regression analysis to develop Eq. (4.12) for the time of arrival of the centroid 52

Fig. 4.4. Comparison of the tracer response curves predicted by the proposed, ADE, and Jobson methods to measured concentrations. 53

Fig. 4.5. Histograms of the ratio of the predicted and measured arrival times of the leading edge: (a) proposed method, (b) ADE method, and (c) Jobson method. The fraction ϕ is taken to be 0.1. The data for the measured times and ADE and Jobson estimates were retrieved from Rehmann (2015)..... 54

Fig. 4.6. Histograms of the ratio of the predicted and measured arrival times of the trailing edge: (a) proposed method, (b) ADE method, and (c) Jobson method. The fraction ϕ is taken to be 0.1. The data for the measured times and ADE and Jobson estimates were retrieved from Rehmann (2015)..... 55

Fig. 4.7. Histograms of the ratio of the predicted and measured arrival times of the peak concentration: (a) proposed method and (b) Jobson method. The data for the measured times and Jobson estimates were retrieved from Rehmann (2015). 56

Fig. 4.8. Histograms of the ratio of the predicted to measured peak concentration: (a) proposed method and (b) Jobson method. The data for the measured times and Jobson estimates were retrieved from Rehmann (2015)..... 57

LIST OF TABLES

Page

Table 4.1. River discharge and drainage area data collected from USGS gaging stations. 48

NOMENCLATURE

A	cross sectional area of the river channel;
a	location parameter for Gumbel distribution;
b	scale parameter for Gumbel distribution;
C	concentration;
C_0	initial concentration;
C_1	concentration in flowing zone;
C_2	concentration in stagnant zone;
c_m, c_s, c_h	concentrations in the main channel, surface storage and hyporheic zone, respectively;
C_m, C_s, C_h	dimensionless concentrations in the main channel, surface storage and hyporheic zone, respectively;
C_{m1}, C_{m2}, C_{m3}, C_{m4}	components of the concentration C_m;
C_p	peak concentration;
C_{pm}	measured peak concentration;
C_{pp}	predicted peak concentration;
CSK_m	skewness coefficient for the main channel;
D_a	drainage area;
D_x	streamwise mixing coefficient;
D_y	transverse mixing coefficient;
E_s	transfer coefficient between surface storage and main channel;
E_h	transfer coefficient between subsurface storage and main channel;

F	general function;
F_{nt}	nth temporal moment in the flowing zone;
F_{nx}	nth spatial moment in the flowing zone;
$\tilde{F}$	Laplace transform of function F;
$f(x,t)$	function in formula for C_1 and C_2 for maintained injection case;
g	acceleration of gravity;
g_m	numerator of temporal skewness coefficient for main channel;
g_s	numerator of temporal skewness coefficient in the surface storage;
g_{tf}	numerator of temporal skewness coefficient in the flowing zone;
g_{tm}	numerator of temporal skewness coefficient for the entire channel;
g_{ts}	numerator of temporal skewness coefficient in the stagnant zone;
g_{xm}	numerator of spatial skewness coefficient for the entire channel;
$g(x,\tau)$	function in the integrals;
$H(z)$	Heaviside step function;
$I_1(z)$	modified Bessel function of first kind and order 1;
j	zone index;
K	dispersion coefficient;
Kr	kurtosis;

K_∞	α^2U^2/β, asymptotic dispersion coefficient in R&W model;
L	the distance from injection site to measurement site;
L_a	advective length;
L_t	transverse length;
M	initial mass of tracer injected;
M_n	nth temporal moment for entire channel;
M_{nt}	nth temporal moment for entire channel;
M_{nx}	nth spatial moment for entire channel;
n	order of moment;
p	$(1-\alpha)s+\beta-\beta^2/(\alpha s+\beta)$;
Q	discharge;
Q_a	mean annual discharge;
S	channel slope;
S_{nt}	nth temporal moment in stagnant zone;
S_{nx}	nth spatial moment in stagnant zone;
s	Laplace transform variable;
T	dimensionless time;
T_1, T_2, T_3	auxiliary time variables;
t	time;
t_L, t_P, t_T	arrival times of the leading edge, the peak concentration and the trailing edge respectively;
t_{Lm}, t_{Pm}, t_{Tm}	measured arrival times of the leading edge, the peak concentration and the trailing edge, respectively;

t_{Lp}, t_{Pp}, t_{Tp}	arrival times of the leading edge, the peak concentration and the trailing edge, respectively;
w_0 ,w_1, w_2	empirical coefficients to compute area of the river cross section
U	mean velocity;
x	streamwise coordinate;
x'	$D_y x/(UB^2)$
X	dimensionless streamwise coordinate;
α	fraction of channel width occupied by stagnant zone;
α_s	the ratio of the surface storage area to main channel area;
α_h	the ratio of the hyporheic storage area to main channel area;
β_s	dimensionless transfer coefficient between surface storage and main channel;
β_h	dimensionless transfer coefficient between hyporheic storage and main channel;
ε	K/UL, inverse of the Peclet number;
$\delta(z)$	Dirac delta function;
γ_t	skewness coefficient;
γ_{tf}	temporal skewness coefficient in flowing zone;
γ_{xf}	spatial skewness coefficient in flowing zone;
γ_{xm}	spatial skewness coefficient for entire channel;
Γ	$\beta_s + \beta_h + q + \lambda_m$
Γ_h	$(\beta_h + \lambda_h)/\alpha_h$

Γ_s	$(\beta_s + \lambda_s)/\alpha_s$
μ_m	time of arrival of centroid for entire channel;
μ_s	time of arrival of centroid in surface stotrage;
μ_t	time of arrival of centroid;
μ_{tf}	time of arrival of centroid in flowing zone;
μ_{tm}	time of arrival of centroid for entire channel;
μ_{ts}	time of arrival of centroid in stagnant zone;
μ_{xm}	position of centroid for entire channel;
ϕ	fraction of the peak used to compute the cloud's edges;
θ	empirical exponent to account for effects of dispersion on travel time;
σ_m^2	temporal variance for main channel;
σ_s^2	temporal variance in surface storage;
σ_{tf}^2	temporal variance in flowing zone;
σ_{tm}^2	temporal variance for entire channel;
σ_{ts}^2	temporal variance in stagnant zone;
σ_{xm}^2	spatial variance for entire channel;
τ, τ_1, τ_2	integration variables;

ACKNOWLEDGMENTS

I would like to acknowledge that the Ministry of National Education of Turkey has financially supported me throughout my graduate studies here in the United States. I would also like to thank the Department of Civil, Construction, and Environmental Engineering for allowing me to be a part of the Iowa State community.

My special and heartfelt thanks go to my advisors Drs. Halil Ceylan and especially Chris Rehmann, who is my academic father and mentor. I learned a lot by working with him. I also would like to thank Drs. Say Kee Ong, Roy Gu, and Kristie Franz for serving on my dissertation committee and giving me feedback.

I would also acknowledge my fellow colleagues Dr. Cynthia Maroney, Lauren Schwab, Yuqi Song, Ian Willard and Zhimin Li. I had great pleasure working with them under Dr. Rehmann's supervision. Additional thanks go to Dr. David Green and David Dziubanski, with whom I had a chance to take courses together and have nice conversations.

ABSTRACT

To improve predictions of contaminant transport in rivers, two analytical models and one empirical model were evaluated. Analytical solutions of the model of Reichert and Wanner (1991), which represents mixing in the advective zone by dividing the channel into a flowing zone and a stagnant zone, were developed for two cases: a spill in the stagnant zone and a maintained injection in the flowing zone. Compared to the case of a flowing zone spill solved by Schmalle and Rehmann (2014), contaminant clouds for a stagnant zone spill travel more slowly, spread more, and shift from positive to negative skewness. These differences are due to the initial delay in advection of the cloud caused by transfer from the stagnant zone to the flowing zone. The solution for a maintained injection in the flowing zone differs from that from the ADE only for small times and distances from the source. This study provides further solutions to be used as building blocks in constructing more complex solutions for contaminant transport in the advective zone of a river.

The second model introduces an analytical solution for a transient storage model that accounts for surface storage and hyporheic exchange as well as for lateral inflow and decay in the main channel and two storage zones. Analysis of temporal moments shows that the subsurface storage zone affects the transport even if the transfer coefficient between subsurface storage and the main channel is two orders of magnitude smaller than the transfer coefficient for surface storage. The analytical solution for the two-storage model is not only practical but it also avoids the challenges of modifying and calibrating the existing numerical model that accounts for only one storage zone.

To avoid the challenges of estimating the parameters for mixing models from limited data about the flow, an empirical model was developed that uses data readily available at

gaging stations operated by the U.S. Geological Survey (USGS). The empirical model represents the tracer response with the Gumbel distribution, which has a skewness coefficient close to the value observed in tracer studies. The proposed model predicts arrival times of the leading and trailing edge better than a similar method developed by the USGS, and it underestimates the peak concentration by an average of 17%. The proposed method mimics the non-Fickian behavior of the transport observed in rivers while avoiding the computational cost and data requirements of more complex models.

CHAPTER 1. INTRODUCTION

Significance and Problem Definition

Many municipalities across the United States rely on rivers as a primary source of drinking water (Waldon 1998), and a leak or spill of toxic chemicals is an ever-present danger both to the river and to downstream municipalities. Such a dramatic spill occurred in Charleston, WV in 2014. Crude 4-methylcyclohexanemethanol (MCHM), a highly toxic chemical used in coal mining, leaked from a chemical plant near the Elk River approximately 1.6 km upstream of the water intake for the Charleston, WV metropolitan area. This spill affected almost 300,000 people and left them without access to drinking water for more than a week (Mistich 2017). In addition to chemical plants located near rivers, thousands of gallons of chemicals are transported on highways and railroads every day, and accidents on highways or railroad bridges are almost inevitable. After a Canadian National rail accident at a bridge over the Cheakamus River north of Vancouver, British Columbia, 41,000 L of a highly toxic chemical was released into the river and affected the biota in the river and surrounding areas (Rivord et al. 2014). Forecasting and responding to such spills requires efficient and reliable methods for predicting contaminant transport.

To predict the concentration C of a contaminant as a function of time t and distance x, the one-dimensional advection dispersion equation (ADE)

$$\frac{\partial C}{\partial t} + U\frac{\partial C}{\partial x} = K\frac{\partial^2 C}{\partial x^2} \tag{1.1}$$

is commonly used (Schmalle and Rehmann 2014). The ADE results from the shear dispersion theory of Taylor (1954), and it requires only two parameters: the mean velocity U and the dispersion coefficient K. The simplicity and attractiveness of the ADE comes with

some limitations. For example, the ADE applies only when the tracer or the contaminant is fully mixed across the river channel, or, in other words, beyond the advective zone. The length of the advective zone can be small for creeks, narrow rivers, and irrigation canals and large for wider channels, ranging from meters to hundreds of kilometers (Schmalle and Rehmann 2014). In the advective zone, Taylor's dispersion theory does not apply, and a different model is needed.

A few models address contaminant transport in the advective zone of a river but, because of the complexity of transport near the source, some either require a great deal of information about the flow (Boxall and Guymer 2003; Zhang 2011) or need to be calibrated for dispersion (Pagsuyoin et al. 2012). A relatively simple model that separates the river channel into two sections—a flowing zone and a stagnant zone—was proposed by Reichert and Wanner (1991) and solved analytically by Schmalle and Rehmann (2014). This model predicts concentrations better than the ADE, but the only available analytical solution focuses on the case of instantaneous injection in the flowing zone. To construct more general solutions for transport in the advective zone, this model needs to be evaluated for a greater range of contaminant transport scenarios.

Although ADE becomes applicable once the contaminant or tracer has passed the advective zone, tracer studies have shown that tracer response curves are more skewed and long-tailed than the Gaussian distribution predicted by the ADE. Over long distances the contaminant experiences disturbances such as pools, riffles, boulders, debris, and recirculation zones in the river channel, and it can interact with ground water. These factors cause tracer response curves to be skewed and long-tailed (Nordin and Troutman 1980). A model that attempts to predict the non-Gaussian behavior of the tracer response curves and

account for the aforementioned factors is the transient storage model (TSM) (Bencala and Walter 1983; Nordin and Troutman 1980). The TSM resembles the ADE but adds the element of exchange between the main channel and a storage zone.

While the TSM produces much better results than the ADE (Deng et al. 2004), detailed tracer studies have shown that the transfer rate between the main channel and surface storage zone differs from the transfer rate between the main channel and the subsurface, with faster exchange occurring at the surface and slower exchange occurring within the subsurface. The greater residence time in the subsurface can affect the chemical behavior of the contaminant (Choi et al. 2000), so Choi et al. (2000) and Phanikumar et al. (2007) suggest separating the transfer at the surface and the transfer within the subsurface by introducing a second storage zone into the TSM.

Tracer studies have been modeled with a modified version of the One-Dimensional Transport with Inflow and Storage (OTIS) package that was originally designed for onestorage zone (Runkel 1998). Although OTIS can be conveniently used for a prescribed mass flux varying with time, it must be calibrated for instantaneous slug releases by defining upper boundary conditions that vary with time (De Smedt et al. 2005). To avoid challenges of modifying OTIS and calibrating it to instantaneous slug releases, an analytical model for a two-storage TSM is needed.

Despite the fact that the TSM and the advective zone model are reliable and efficient methods for analyzing contaminant transport in rivers, the parameters involved in these models are most reliably determined in tracer experiments whose results apply only to specific flow conditions at the time of the experiment. Also, conducting detailed tracer studies to estimate model parameters is not cost-effective. To avoid the challenges of

estimating the parameters involved in other mixing models, Jobson (1997) introduced a method to estimate travel times and concentrations of a contaminant using only the discharge, the mean annual discharge, the drainage area, and the slope of a river. Although Jobson's approach is easy to use, it has shortcomings arising from its simplicity. For example, the method does not account for the constant skewness coefficient of 1.18 observed in measured tracer response curves (Gonzalez-Pinzon et al. 2013). To improve predictions of contaminant transport with limited data, a method that accounts for constant skewness is needed.

Objectives

The overall objective of this research is to develop models that can be used to predict contaminant transport.

1) The objective of Chapter 2 is to expand the analytical solutions available for constructing solutions for contaminant transport in the advective zone. Solutions using the model of Reichert and Wanner (1991) will be presented for a contaminant spill that occurred in the non-flowing section of a river and maintained pollution in the flowing section of a river.
2) The objective of Chapter 3 is to develop an analytical solution using a transient storage model with two storage zones that accounts for lateral inflow and decay in the main channel as well as in the storage zones.
3) The objective of Chapter 4 is to develop empirical relationships that can be used to predict tracer response curves that produce improved estimates of travel time and concentrations and maintain the persistent skewness observed in the field.

Organization of the Dissertation

The following chapters discuss improvements to models of contaminant transport. A model for predicting contaminant concentrations near the source is developed in Chapter 2. Chapter 3 focuses on a model that accounts for two storage zones, lateral inflow, and decay in predicting contaminant transport farther downstream. Chapter 4 presents an empirical model that accounts for the persistent skewness observed in tracer-response curves measured in field experiments. Conclusions and possible future studies are described in Chapter 5.

References

Bencala, K. E., and R. A. Walter (1983), Simulation of solute transport in a mountain oil-and-riffle stream with a kinetic mass transfer model, *Water Resources Research*., 19(3), 718–724.

Boxall, J. B., and I. Guymer (2003), Analysis and prediction of transverse mixing coefficients in natural channels, *Journal of Hydraulic Engineering*, 129(2), 129–139, doi:10.1061/(ASCE)0733-9429(2003)129:2(129).

Choi, J., J. W. Harvey, and M. H. Conklin (2000), Characterizing multiple timescales and storage zone interaction that affect solute fate and transport in drainage basin, *Water Resources Research*., 36(6), 1511–1518.

Deng, Z. Q., V. P. Singh, and L. Bengtsson (2004), Numerical solution of fractional advection-dispersion equation, *Journal of Hydraulic Engineering*, 130(5), 422–431, doi:10.1061/(ASCE)0733-9429(2004)130:5(422).

Gonzalez-Pinzon, R., R. Haggerty, and M. Dentz (2013), Scaling and predicting solute transport processes in streams, *Water Resources. Research*., 49(7), 4071–4088, doi:10.1002/wrcr.20280.

Jobson, H. E. (1997), Predicting travel time and dispersion in rivers and streams, *Journal of Hydraulic Engineering*, 123(11), 971–978.

Mistich, D. (2017), Federal judge reviews $151 million chemical spill settlement, *Associated Press*. Available from: http://wvpublic.org/post/federal-judge-reviews-151-million-chemical-spill-settlement

Nordin, C. F., and B. M. Troutman (1980), Longitudinal dispersion in rivers: The persistence of skewness in observed data, *Water Resources Research*., 16(1), 123–128.

Pagsuyoin, S. A., W.-S. Lung, and L. M. Colosi (2012), Predicting EDC concentrations in a river mixing zone, *Chemosphere*, 87(10), 1111–1118, doi:http://dx.doi.org/10.1016/j.chemosphere.2012.02.004.

Phanikumar, M. S., I. Aslam, C. Shen, D. T. Long, and T. C. Voice (2007), Separating surface storage from hyporheic retention in natural streams using wavelet decomposition of acoustic Doppler current profiles, *Water Resources Research*, 43(5), 1–16, doi:10.1029/2006WR005104.

Reichert, P., and O. Wanner (1991), Enhanced one-dimensional modeling of transport in rivers, *Journal of Hydraulic Engineering*, 117(9), 1165–1183, doi:10.1061/(ASCE)0733-9429(1991)117:9(1165).

Rivord, J., L. Saito, G. Miller, and S. S. Stoddard (2014), Modeling contaminant spills in the Truckee River in the western United States, *Journal of Water Resources Planning and Management*, 140(3), 343–354, doi:10.1061/(ASCE)WR.1943-5452.0000338.

Runkel, R. L. (1998), One-dimensional transport with inflow and storage (OTIS): a solute transport model for streams and rivers, Denver, Colorado.

Schmalle, G., and C. Rehmann (2014), Analytical solution of a model of contaminant transport in the advective zone of a river, *Journal of Hydraulic Engineering*, 140(7), 4014029, doi:10.1061/(ASCE)HY.1943-7900.0000885.

De Smedt, F., W. Brevis, and P. Debels (2005), Analytical solution for solute transport resulting from instantaneous injection in streams with transient storage, *Journal of Hydrology*, 315(1–4), 25–39, doi:10.1016/j.jhydrol.2005.04.002.

Taylor, G. (1954), The dispersion of matter in turbulent flow through a pipe, *Proceedings of the Royal Society of London*, A223, 446–468, doi:10.1098/rspa.1983.0054.

Waldon, M. G. (1998), Time-of-travel in the lower Mississippi River: model development, calibration, and application, *Water Environment Research*, 70(6), 1132–1141, doi:10.2175/106143098X123499.

Zhang, W. (2011), A 2-D numerical simulation study on longitudinal solute transport and longitudinal dispersion coefficient, *Water Resources Research*, 47(7), 1–13, doi:10.1029/2010WR010206.

CHAPTER 2. FURTHER ANALYTICAL SOLUTIONS FOR CONTAMINANT TRANSPORT IN THE ADVECTIVE ZONE OF A RIVER

A paper to be submitted to the *Journal of Hydraulic Engineering*

Rusen Sinir, Chris Rehmann, and Halil Ceylan

Abstract

To address limitations of the one-dimensional advection-dispersion equation (ADE) in describing the advective zone of a river, analytical solutions for two more cases of a model proposed by Reichert and Wanner (1991) for advective zone contaminant transport are obtained and evaluated. The governing equations of the model, which divides the river channel into a flowing zone and a stagnant zone, are solved for the case of a spike injected into the stagnant zone of a river channel and for the case of maintained injection, where concentration at a point in the flowing zone is held constant. Compared to the case of a flowing zone spill, contaminant clouds for a stagnant zone spill travel more slowly, spread more, and shift from positive to negative skewness. These differences are due to an initial delay in advection of the cloud caused by transfer from the stagnant zone to the flowing zone. The solution for a maintained injection in the flowing zone differs from that obtained from the ADE only at small times and distances from the source. The present study provides further solutions to be used as building blocks in constructing more complex solutions for contaminant transport in the advective zone of a river.

Introduction

The one-dimensional advection dispersion equation (ADE) has been extensively studied and applied to numerous problems in river mixing under different conditions to estimate concentrations of contaminants after spills. Although the ADE approach is attractive

and easy to implement, it is limited to the far field, and it does not apply unless a balance between differential advection and transverse mixing is reached (Fischer et al. 1979; Taylor 1954). The required distance can range from as small as 10 m in narrow streams to 1000 m in large rivers (Schmalle and Rehmann 2014). Hence, better models for estimating contaminant transport in the advective zone of a river are needed.

To improve the accuracy of the estimates, several studies have used two- or three-dimensional versions of the ADE to deal with the complexity of near-field processes (Pagsuyoin et al. 2012; Ye and McCorquodale 1996; Zhang 2011). For example, Pagsuyoin et al. (2012) used a two-dimensional model that accounts for advection and spreading in the *x*- and *y*-directions only. Because this model does not account for dispersion, spreading coefficients must be calibrated. Another two-dimensional model by Zhang (2011), which accounts for eddy diffusivities requires a great deal of additional information and computational effort. Knowledge of the detailed velocity distribution allows dividing the river channel into multiple stream tubes (Boxall and Guymer 2003), but that approach increases the complexity of the predictions.

Reichert and Wanner (1991, hereafter referred to as R&W) proposed a model to capture key elements of the transport in the near field such as arrival time of the centroid and peak concentration. The model divides the river channel into a flowing zone and a stagnant zone. The fraction of the channel occupied by the stagnant zone is α. The flowing zone velocity is $U/(1-\alpha)$, whereas the stagnant zone has zero velocity. Transfer between the two zones is controlled by the transfer coefficient β. The governing equations for the contaminant concentrations C_1 for the flowing zone and C_2 for the stagnant zone are given as

$$(1-\alpha)\frac{\partial C_1}{\partial t}+U\frac{\partial C_1}{\partial x}=-\beta\left(C_1-C_2\right) \tag{2.1}$$

$$\alpha \frac{\partial C_2}{\partial t} = \beta \left(C_1 - C_2 \right) \tag{2.2}$$

where t is time and x is the streamwise coordinate. Because R&W did not disclose their solution method, Schmalle and Rehmann (2014) introduced an analytical solution to avoid challenges of numerically solving hyperbolic partial differential equations and to increase the accuracy and the effectiveness of the model.

The R&W model produces better results than the one-dimensional ADE for concentrations in the advective zone with less information and effort than two- or three-dimensional models require (Schmalle and Rehmann 2014). The case when instantaneous injection occurs in the flowing zone was studied and understood well by R&W and Schmalle and Rehmann (2014). They found that (1) increasing the stagnant zone fraction α decreases the peak concentration and increases the spread of the cloud and (2) increasing transfer coefficient β causes an increase in the peak concentration and a decrease in the spread of the cloud. They also discussed that narrow initial pulses cause an additional pulse to occur on the tracer response curves. Schmalle and Rehmann (2014) also gave analytical expressions for estimating the parameters (U, α, β) involved in the governing equations from measurements.

Although the solution of Schmalle and Rehmann (2014) allows solutions for other types of contaminant injections in the flowing zone to be constructed using superposition, it does not address injections into the stagnant zone. To be able to construct additional solutions for estimating concentrations in the advective zone, the objective of this study was to investigate two more cases: (1) an instantaneous injection into the stagnant zone and (2) a maintained injection into the flowing zone. The solutions are derived in the next section, and the results for tracer-response curves and spatial moments are presented in the following

section. After the behavior of spatial moments and concentration curves are discussed, conclusions are presented.

Methods

The solution of the system of Eqs. (2.1) and (2.2) for a spill in the stagnant zone proceeds by applying a Laplace transform in time and solving the system of ordinary differential equations (ODEs) in space . The initial conditions for the system of equations for spill in the stagnant zone case are that there is no contaminant in the flowing zone—i.e., $C_1(x,0)=0$—and there is an instantaneous injection (spike) into the stagnant zone: $C_2(x,0) = (M/\alpha A)\delta(x)$, where M is the initial mass of the spill, A is the cross-sectional area of the river channel, and $\delta(x)$ is the Dirac delta function.

The Laplace transform of concentrations in zone j is given by

$$L\left[C_j\left(x,t\right)\right]=\tilde{C}_j\left(x,s\right)=\int_0^\infty e^{-st}C_j\left(x,t\right)dt \tag{2.3}$$

Upon applying the Laplace transform to Eq.(2.2), one can obtain $\tilde{C}_2\left(x,s\right)$ as

$$\tilde{C}_2\left(x,s\right)=\frac{\beta}{\alpha s+\beta}\tilde{C}_1\left(x,s\right)+\frac{\alpha}{\alpha s+\beta}C_2\left(x,0\right) \tag{2.4}$$

$\tilde{C}_2$ can then be eliminated from the transformed form of Eq. (2.2) for $\tilde{C}_1$ using Eq. (2.4) to obtain a first order ODE

$$U\frac{\partial\tilde{C}_1}{\partial x}+\left[\left(1-\alpha\right)s+\beta-\frac{\beta^2}{\alpha s+\beta}\right]\tilde{C}_1=\left(1-\alpha\right)C_1\left(x,0\right)+\frac{\alpha\beta}{\alpha s+\beta}C_2\left(x,0\right) \tag{2.5}$$

The solution of Eq. (2.5) with the given boundary conditions and for the case of no transfer between zones ($\beta = 0$) is

$$\tilde{C}_1(x,s) = \frac{M\beta}{AU(\alpha s+\beta)} e^{-\frac{p}{U}x} \tag{2.6}$$

where $p = (1-\alpha)s + \beta - \dfrac{\beta^2}{\alpha s+\beta}$. One can then obtain $\tilde{C}_2(x,s)$ by substituting Eq. (2.6) into Eq. (2.4)

$$\tilde{C}_2(x,s) = \frac{M\beta^2}{AU(\alpha s+\beta)^2} e^{-\frac{p}{U}x} \tag{2.7}$$

The convolution theorem allows the concentrations in the flowing and stagnant zones to be expressed as

$$C_1(x,t) = \frac{M\beta}{AU\alpha} e^{-\frac{\beta}{U}x} \left(e^{-\frac{\beta}{\alpha}\left(t-(1-\alpha)\frac{x}{U}\right)} \left\{ H\left(t-(1-\alpha)\frac{x}{U}\right) + \int_0^t g(x,\tau)\,d\tau \right\} \right) \tag{2.8}$$

$$C_2(x,t) = \frac{M\beta^2}{AU\alpha^2} e^{-\frac{\beta}{U}x} \left(e^{-\frac{\beta}{\alpha}\left(t-(1-\alpha)\frac{x}{U}\right)} \left\{ \begin{array}{l} H\left[t-(1-\alpha)\frac{x}{U}\right]\left(t-(1-\alpha)\frac{x}{U}\right) \\ +\int_0^t \left(t-\tau-(1-\alpha)\frac{x}{U}\right) g(x,\tau)\,d\tau \end{array} \right\} \right) \tag{2.9}$$

where

$$g(x,\tau) = H\left(t-\tau-(1-\alpha)\frac{x}{U}\right)\frac{\beta}{\alpha}\sqrt{\frac{x\alpha}{U\tau}} I_1\left(2\beta\sqrt{\frac{x\tau}{U\alpha}}\right) \tag{2.10}$$

where $H(z)$ is the step function and $I_1(z)$ is the modified Bessel function of the first kind and the first order.

The solution of the system of Eqs. (2.1) and (2.2) for maintained pollution in the flowing zone follows the same procedure used for the spill in the stagnant zone. In the case of maintained pollution, the concentration at $x = 0$ is held constant at C_0 ($C_1(0,t) = C_0$), and the river channel is initially clean everywhere ($C_1(x,0) = 0$). The solution of Eq. (2.5) is

$$\tilde{C}_1(x,s) = \frac{C_0}{s} e^{-\frac{p}{U}x} \tag{2.11}$$

and from Eq. (2.4)

$$\tilde{C}_2(x,s) = \frac{C_0 \beta}{s(\alpha s + \beta)} e^{-\frac{p}{U}x} \tag{2.12}$$

Inverting the transforms gives

$$C_1(x,t) = C_0 e^{-\frac{\beta}{U}x} f_1(x,t) \tag{2.13}$$

$$C_2(x,t) = C_0 e^{-\frac{\beta}{U}x} \left[f_1(x,t) - e^{-\frac{\beta}{\alpha}\left(t-(1-a)\frac{x}{U}\right)} \left\{ H\left[t-(1-a)\frac{x}{U} \right] + \int_0^t g(x,\tau)\, d\tau \right\} \right] \tag{2.14}$$

where

$$f_1(x,t) = H\left[t-(1-\alpha)\frac{x}{U} \right] + \int_0^t e^{-\frac{\beta\tau}{\alpha}} g(x,\tau) d\tau \tag{2.15}$$

Computing the concentrations requires numerically evaluating the integrals in Eqs. (2.8) and (2.9) because they do not have closed-form solutions. To reduce computational cost and increase accuracy of the integrals, Gaussian quadrature is used.

Computing spatial and temporal moments provides an understanding of how bulk quantities such as the mass, position of the centroid, and skewness behave and helps to determine the parameters involved in the model from field measurements (Schmalle & Rehmann 2014). To compute spatial and temporal moments, the approach presented by Schmalle and Rehmann (2014) is followed. Results are listed in the Appendix.

Results

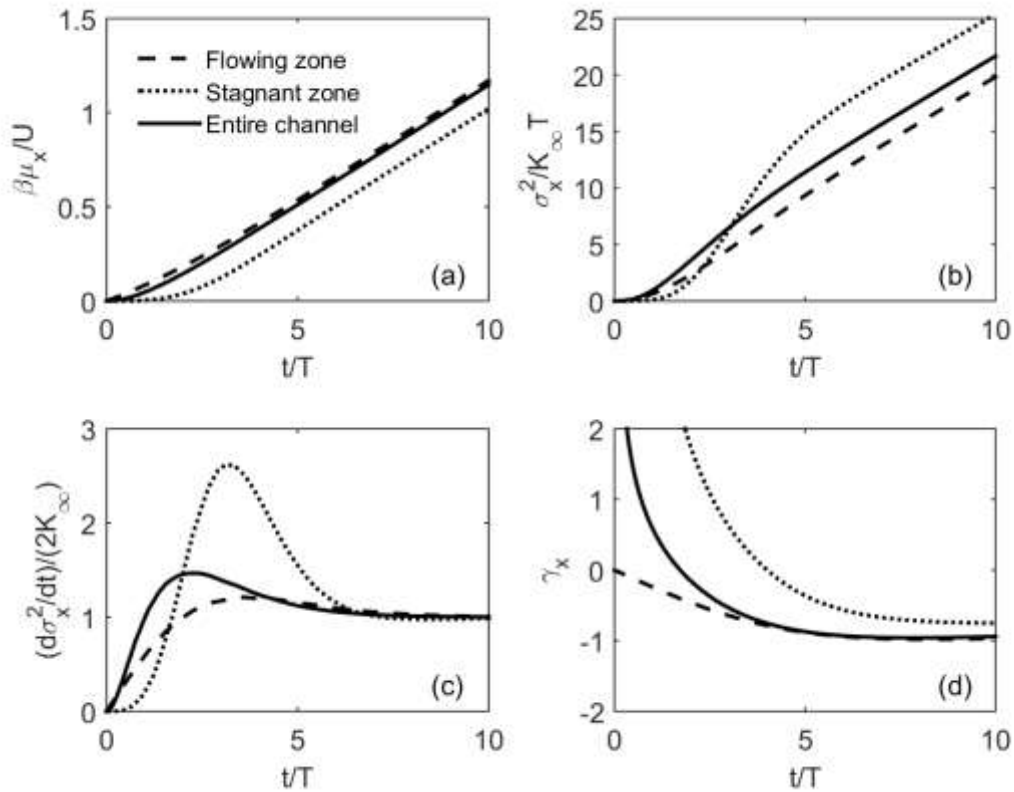

Fig. 2.1. Evolution of parameters computed from spatial moments: (a) position of the centroid; (b) variance; (c) rate of change of the variance; (d) skewness. Results are computed for $\alpha = 0.15$.

At large times the spatial moments in flowing and stagnant zones behave similarly, but at small times the behavior differs (Fig. 2.1). At small times ($t/T < 3$, where $T = \alpha(1-\alpha)/\beta$), although the centroid for the stagnant zone moves quite slowly, the centroid for the flowing zone and centroid for the entire channel move at a speed slightly less than U [Fig. 2.1(a)]. The variance for the stagnant zone behaves differently from the variances for the flowing zone and the entire channel at small times ($t/T < 6$). For $t/T < 2$, the variance for the stagnant zone is less than those for the entire channel and the flowing zone and it grows faster for $1 < t/T < 3$ [Fig. 2.1(b)]. The rate of growth of variance for stagnant zone increases

well above $2K_\infty$ and begins to decrease after t/T=3 (Fig. 2.1(c)). The skewness coefficient for the stagnant zone is initially zero because of the initial condition of a spike. For $t/T < 2$, it is extremely large because the spike takes time to develop a Gaussian-like distribution. As time increases, values of the skewness coefficient for the stagnant zone, the flowing zone, and the entire channel all approach zero. This is expected because of the asymptotic behavior of the model as either time or distance downstream increases [Fig. 2.1(d)].

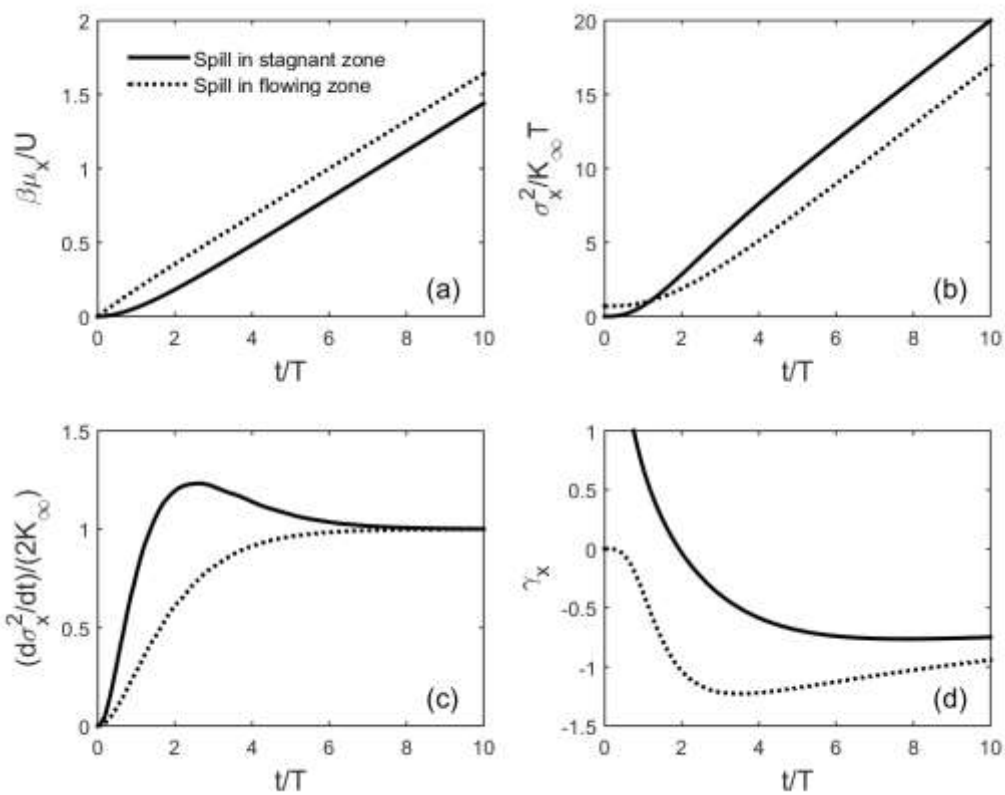

Fig. 2.2. Comparison of the spatial moments for a spill in the stagnant zone and a spill in the flowing zone.

Because of the asymptotic behavior of the R&W model, the behavior of the spatial moments for the cases of a spill in the flowing zone and a spill in the stagnant zone have similarities after sufficient time has elapsed. Spatial moments of the entire channel for both

cases were computed to compare their behavior. At early times (about $t/T < 2$), the centroid for a spill in the stagnant zone moves more slowly than the centroid for a spill in the flowing zone [Fig. 2.2(a)]. The variance for a spill in the stagnant zone is larger than the variance for a spill in the flowing zone [Fig. 2.2(b)], and the rate of growth for a spill in the stagnant zone case is larger than the growth rate of a spill in the flowing zone case until they both approach $2K_\infty$ [Fig. 2.2(c)]. At early times, the skewness for a spill in the stagnant zone is positive, while it is negative for a spill in the flowing zone [Fig. 2.2(d)].

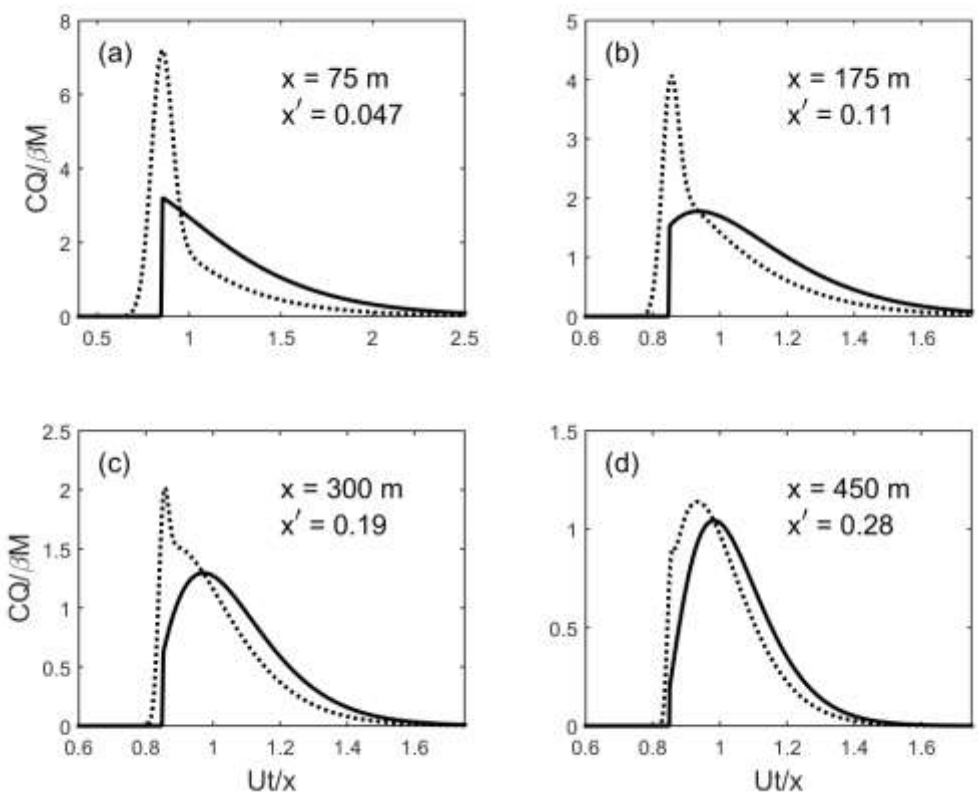

Fig. 2.3. Comparison of tracer-response curves for a spill in the stagnant zone (solid line) and a spill in the flowing zone (dotted line). The initial mass is the same.

Tracer-response curves for the cases of spills in the flowing and stagnant zones differ near the source but approach one another farther downstream (Fig. 2.3). The comparison involves an initial Gaussian pulse for the case of a spill in the flowing zone, as in Schmalle and Rehmann (2014), and an initial spike for the case of a spill in the stagnant zone; the cases have the same initial mass. For $x' = D_y x/(UB^2) < 0.08$, where the model should not apply (R&W), the shapes of the curves for the two cases are quite different. The curve for the stagnant zone injection exhibits a sharp front and a long tail, while the concentrations for the flowing zone injection reach a peak value greater by more than a factor of 2. The sharp front for the stagnant zone injection remains visible throughout the advective zone, though by $x' = 0.28$ it is small. As Schmalle and Rehmann (2014) discuss in detail, a narrow initial pulse can lead to a separate pulse in the tracer-response curves for the case of spill in the flowing zone. On the other hand, a spill in the stagnant zone case does not yield a separate pulse in downstream concentrations.

Except for small times and small distances from the source, the R&W model applied to a maintained injection in the flowing zone yields results similar to those predicted with the ADE (Fig. 2.4). The main difference is the arrival of the contaminant at the measurement site. While the ADE predicts a smooth increase from zero in concentration, the R&W model yields a sharp jump in concentration. Differences between the predictions of the two models are largest for small values of x'. By $x' = 0.28$, the predictions are nearly identical, but even for small values of x', the concentrations are close for $Ut/x > 1$.

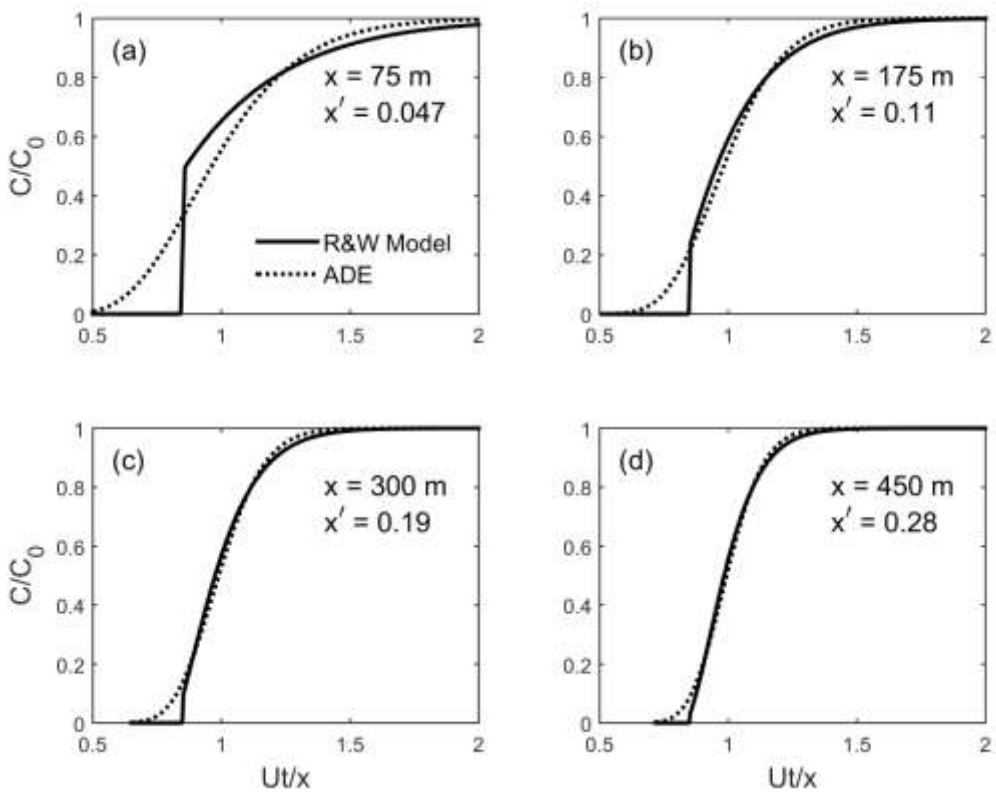

Fig. 2.4. Comparison of R&W model and ADE for the case of a maintained injection in the flowing zone. Results are computed for $\alpha = 0.15$, $\beta = 4.5 \times 10^{-3}$ s^{-1}, and $U = 0.6$ m/s.

Discussion

Differences arise in the spatial moments between the case with a flowing zone injection and the case with a stagnant zone injection because of initial movement of the tracer cloud. In the case of a spill in the flowing zone, the cloud begins moving downstream and exchanging with the stagnant zone immediately, while in the case of spill in the stagnant zone, the cloud first transfers from the stagnant zone to the flowing zone and then starts moving downstream. Therefore, the centroid for the stagnant zone in the case with a stagnant zone injection moves little at early times [Fig. 2.1(a)], while centroids for a spill in the flowing zone move at a speed closer to U (Schmalle and Rehmann 2014). The majority of the

initial contaminant is transferred to the flowing zone and moving downstream by the time the centroid for the stagnant zone moves at the same rate as the centroid for the flowing zone [Fig. 2.1(a)]. This delay in advection causes the centroid for the entire channel to move slower in the case of a stagnant zone spill than the centroid for the entire channel for a flowing zone spill [Fig. 2.2(a)].

Differences in behavior caused by initial conditions can be observed for higher moments as well. For a flowing zone spill the variance for the stagnant zone always exceeded the variances for both the flowing zone and the entire channel (Schmalle and Rehmann 2014). For a stagnant zone spill, however, the variance for the stagnant zone is less than variances for the flowing zone and the entire channel at small times and then rapidly increases and becomes larger than variances for the flowing zone and the entire channel [Fig. 2.1(b)]. This rapid increase arises because, although most of the contaminant is being transported downstream, a small amount remains at the injection site. In a similar way, the skewness differs between the flowing zone injection and the stagnant zone injection. In the former case, in which the cloud begins moving immediately, the skewness is negative throughout the advective zone (Schmalle and Rehmann 2014). In the latter case, because downstream concentrations are less than upstream concentrations at small times, the skewness coefficient for the stagnant zone is positive; once the bulk of the cloud is moving downstream, the skewness becomes negative [Fig. 2.2(d)].

To compute tracer response curves, the case with stagnant zone injection uses a spike as an initial condition, while the case with flowing zone injection uses a Gaussian pulse with restrictions on the initial width (Schmalle and Rehmann 2014). Having an initial pulse that is too narrow causes an additional pulse to occur in the tracer response curves for the case with

a flowing zone injection (Fig. 2.3), while an additional pulse does not occur in the case with stagnant zone injection even if the initial condition is a spike. The hyperbolic nature of Eq. (2.1) shows that an initial spike will be advected downstream as exchange with the stagnant zone occurs. In contrast, for a stagnant zone injection, advection does not occur until contaminant has transferred from the stagnant zone to the flowing zone. To model a flowing zone injection, recommendations by Schmalle and Rehmann (2014) with respect to the width of the initial Gaussian pulse should be followed to avoid an additional pulse in the tracer response curves.

Although the R&W model outperformed the ADE in predicting measured concentrations in the advective zone of a river for an instantaneous injection (Schmalle and Rehmann 2014), results from the R&W model for a maintained injection in the flowing zone do not differ significantly from the predictions of the ADE (Fig. 2.4). The R&W model predicts a sharp front in the tracer response curve and therefore a later arrival of the contaminant at a measurement site (Fig. 2.4) because it does not account for dispersion. Measurements in the advective zone for a maintained injection are needed to evaluate how well the R&W model predicts compared to the ADE.

The work presented here expands the solutions available for predicting contaminant transport in the advective zone. As Schmalle and Rehmann (2014) discuss, R&W presented examples of predictions of their model but gave no details of the solution method as to whether it was analytical or numerical. The analytical solution of Schmalle and Rehmann (2014) provides a way to estimate concentrations in the advective zone without the cost and effort of a numerical solution, but it is limited to a flowing zone injection. The present study

fills this gap by providing further analytical solutions that can be used to construct solutions for other injection types using superposition, as in Fischer et al. (1979, ch. 2).

Conclusions

To estimate contaminant transport in the advective zone of a river and construct useful solutions for different scenarios of contamination in rivers, the model proposed by Reichert and Wanner (1991) was solved analytically using Laplace transforms and evaluated for two cases: a spill in the stagnant zone and a maintained injection in the flowing zone. The delay in advection of the contaminant cloud caused by transfer from the stagnant zone explains the differences between the solution for a stagnant zone injection and the solution for the flowing zone injection: For the case of stagnant zone injection the centroid of the cloud moves more slowly, the variance is larger, and the skewness starts positive before becoming negative. As R&W showed, far enough downstream all solutions of their model approach the ADE solution. The solution of the R&W model for a maintained injection in the flowing zone is similar to the solution from the ADE; differences appear at small times and distances from the source. This work expands the solutions available for constructing more complex solutions and predicting contaminant transport in the advective zone.

References

Boxall, J. B., and Guymer, I. (2003). “Analysis and prediction of transverse mixing coefficients in natural channels.” *Journal of Hydraulic Engineering*, 129(2), 129–139.

Fischer, H. B., List, E. J., Koh, R. C. Y., Imberger, J., and Brooks, N. H. (1979). Mixing in inland and coastal waters. *Academic*, New York.

Nordin, C. F., and Troutman, B. M. (1980). “Longitudinal dispersion in rivers: The persistence of skewness in observed data.” *Water Resources Research*, 16(1), 123–128.

Pagsuyoin, S. A., Lung, W.-S., and Colosi, L. M. (2012). “Predicting EDC concentrations in a river mixing zone.” *Chemosphere*, 87(10), 1111–1118.

Reichert, P., and Wanner, O. (1991). “Enhanced one-dimensional modeling of transport in rivers.” *Journal of Hydraulic Engineering*, 117(9), 1165–1183.

Schmalle, G.F., and Rehmann, C.R. (2014). “Analytical solution of a model of contaminant transport in the advective zone of a river.” *Journal of Hydraulic Engineering*, 140(7), 4014029.

Sneddon, I. N. (1972). The use of integral transforms. *McGraw-Hill*, New York.

Taylor, G. (1954). “The dispersion of matter in turbulent flow through a pipe.” *Proceedings of the Royal Society of London*, A223, 446–468.

Ye, J., and McCorquodale, J. A. (1996). “Simulation of curved open channel flows by 3d hydrodynamic model.” *Journal of Hydraulic Engineering*, 124(7), 687–698.

Zhang, W. (2011). “A 2-D numerical simulation study on longitudinal solute transport and longitudinal dispersion coefficient.” *Water Resources Research*, 47(7), 1–13.

Appendix. Computation of Spatial and Temporal Moments

Spatial moments are obtained by solving a system of equations derived by multiplying Eqs. (2.1) and (2.2) by x^n and then integrating, as described by Schmalle and Rehmann (2014). The initial conditions for the system of moment equations are all zero except that $S_{0x} = M/\alpha$, where M is the initial mass of contaminant injected per unit area.

$$F_{0x}(t) = M\left(1-\mathrm{e}^{-t/T}\right) \tag{2.16}$$

$$S_{0x}(t) = M\left(1+\frac{(1-\alpha)}{\alpha}\mathrm{e}^{-t/T}\right) \tag{2.17}$$

$$F_{1x}(t) = \frac{MU}{(1-\alpha)\beta}\{\mathrm{e}^{-t/T}[\alpha-3\alpha^2+2\alpha^3-t\alpha\beta]+[3\alpha^2-2\alpha^3-\alpha+t\beta-t\alpha\beta]\} \tag{2.18}$$

$$S_{1x}(t) = \frac{MU}{\beta}\{\mathrm{e}^{-t/T}[2\alpha-2\alpha^2+t\beta]+[2\alpha^2-2\alpha+t\beta]\} \tag{2.19}$$

$$\begin{aligned} F_{2x}(t) = {} & \frac{MU^2}{(1-\alpha)^2\beta^2}\{\mathrm{e}^{-t/T}\alpha^2[2(1-\alpha)^2(1-6(1-\alpha)\alpha)-2t(1-\alpha)(2-3\alpha)\beta+t^2\beta^2]- \\ & (1-\alpha)^2[2\alpha^2(1+6(-1+\alpha)\alpha)-2t\alpha(1-3\alpha)\beta+t^2\beta^2]\} \end{aligned} \tag{2.20}$$

$$\begin{aligned} S_{2x}(t) = {} & \frac{1}{(1-\alpha)\beta^2}MU^2\{(1-\alpha)[6(-1+\alpha)\alpha^2(-1+2\alpha)+2t\alpha(-2+3\alpha)\beta+t^2\beta^2]+ \\ & \mathrm{e}^{-t/T}\alpha[-6\alpha(1-2\alpha)(1-\alpha)^2-2t(1-\alpha)(1-3\alpha)\beta+t^2\beta^2]\} \end{aligned} \tag{2.21}$$

$$\begin{aligned} F_{3x}(t) = {} & \frac{1}{(1-\alpha)^3\beta^3}MU^3\{\mathrm{e}^{-t/T}\alpha^3[6(1-\alpha)^3(1-2\alpha)(1-10(1-\alpha)\alpha)- \\ & 6t(1-\alpha)^2(3-2\alpha(6-5\alpha))\beta+3t^2(1-\alpha)(3-4\alpha)\beta^2-t^3\beta^3]+ \\ & (1-\alpha)^3[6\alpha^3(-1+2\alpha)(1-10(1-\alpha)\alpha)+6t\alpha^2(1-2\alpha(4-5\alpha))\beta- \\ & 3t^2\alpha(1-4\alpha)\beta^2+t^3\beta^3]\} \end{aligned} \tag{2.22}$$

$$S_{3x}(t) = \frac{1}{(1-\alpha)^2 \beta^3} MU^3 \{ \mathrm{e}^{-t/T} \alpha^2 [24(1-\alpha)^3 \alpha (1-5(1-\alpha)\alpha) + 6t(1-\alpha)^2 (1-2\alpha(4-5\alpha))\beta - 6t^2 (1-\alpha)(1-2\alpha)\beta^2 + t^3\beta^3] + (1-\alpha)^2 [-24(1-\alpha)\alpha^3 (1-5(1-\alpha)\alpha) + 6t\alpha^2 (3-2\alpha(6-5\alpha))\beta - 6t^2\alpha(1-2\alpha)\beta^2 + t^3\beta^3]\} \tag{2.23}$$

Temporal moments are computed from Eqs. (2.6) and (2.7) as described by Nordin and Troutman (1980). The arrival time of the centroid μ_t, the temporal variance σ_t^2, and the numerator of the skewness coefficient g_{tf} are computed from the temporal moments. For the flowing zone

$$\mu_{tf}(x) = \frac{x}{U} + \frac{\alpha}{\beta} \tag{2.24}$$

$$\sigma_{tf}^2(x) = \frac{\alpha^2}{\beta}\left(\frac{1}{\beta} + 2\frac{x}{U}\right) \tag{2.25}$$

$$g_{tf}(x) = \frac{2\alpha}{\beta^3}\left(\alpha^2 - 3\alpha(1-2\alpha)\beta\frac{x}{U} - 3(1-\alpha)\beta^2\frac{x^2}{U^2}\right) \tag{2.26}$$

For the stagnant zone

$$\mu_{ts}(x) = \frac{x}{U} + 2\frac{\alpha}{\beta} \tag{2.27}$$

$$\sigma_{ts}^2(x) = 2\frac{\alpha^2}{\beta}\left(\frac{1}{\beta} + \frac{x}{U}\right) \tag{2.28}$$

$$g_{ts}(x) = \frac{2\alpha}{\beta^3}\left(\alpha^2 - 3\alpha(2-3\alpha)\beta\frac{x}{U} - 3(1-\alpha)\beta^2\frac{x^2}{U^2}\right) \tag{2.29}$$

For the entire channel

$$\mu_{tm}(x) = \frac{x}{U} + \frac{\alpha}{\beta} \tag{2.30}$$

$$\sigma_{tm}^{2}\left(x\right)=\frac{\alpha^{2}}{\beta^{2}}\left(1+\alpha+2\beta\frac{x}{U}\right) \tag{2.31}$$

$$g_{tm}\left(x\right)=\frac{2\alpha}{\beta^{3}}\left(\alpha^{2}-3\alpha\left(1-\alpha-\alpha^{2}\right)\beta\frac{x}{U}-3\left(1-\alpha\right)\beta^{2}\frac{x^{2}}{U^{2}}\right) \tag{2.32}$$

CHAPTER 3. ANALYTICAL SOLUTION OF TWO-STORAGE MODEL FOR INSTANTANEOUS SLUG RELEASE

A paper to be submitted to *Journal of Hydraulic Engineering*

Rusen Sinir, Chris Rehmann, and Halil Ceylan

Abstract

An analytical solution of the transient storage model with surface and hyporheic storage zones (2-storage model) in rivers is presented and evaluated as a means for avoiding the challenges of numerical solutions. The analytical solution for a 2-storage model is obtained by utilizing Laplace transform methods for an instantaneous slug release. The solution includes lateral inflow and decay terms that might be useful to those working on nutrient uptake. Analysis of temporal moments shows that the subsurface storage zone affects the transport even if the transfer coefficient between subsurface storage and the main channel is two orders of magnitude smaller than the transfer coefficient for surface storage. Comparison with available data showed the present solution to be as capable of estimating tracer response curves as the numerical package that has been widely used.

Introduction

Transport of contaminants in rivers is affected by the interaction of the contaminant with zones with slowly moving flow such as pools, recirculation zones, vegetated areas, and bed sediment (Bencala 1983; Choi et al. 2000; De Smedt et al. 2005; Wörman et al. 1998). Although the one-dimensional advection-dispersion equation (ADE) is widely used to predict contaminant transport, measurements from tracer experiments show that its ability to estimate concentrations accurately suffers because it cannot represent transport rates smaller than that established by the main channel velocity (Boano et al. 2014). A sound model should

include effects of slower moving compartments of the river if it is to be able to represent transport in natural streams.

To address some of the shortcomings of the ADE, Bencala and Walter (1983) proposed the transient storage model (TSM), which uses first-order exchange to account for interaction of the contaminant with a storage zone such as a recirculation zone,. The TSM requires only two more parameters than the ADE: the ratio of the transient storage zone area to the main channel area and the transfer coefficient between the main channel and the storage zone. The tracer enters a recirculation zone as it passes in the main channel, and after the main cloud moves downstream, the recirculation zone begins releasing contaminant back into the main channel. This slow release causes a long-tailed distribution of contaminant concentrations not well represented by the ADE (Nordin and Troutman 1980). Although the TSM estimates concentrations in the main channel reasonably well (Boano et al. 2014), larger storage time scales caused by sections of the river channel where slow exchange occurs with the main channel are underestimated because exchange parameters depend strongly on the duration of the injection and processes with larger time scales (Bencala et al. 2011; Boano et al. 2014; Wörman et al. 2002).

The standard transient storage model cannot account for both exchange with surface storage zones and hyporheic exchange, the slower exchange happening between the main channel and the subsurface flow (Choi et al. 2000; Wörman et al. 1998; Wörman et al. 2002). Hyporheic exchange occurs in streambed sediments, while surface water interacts with groundwater. Drivers of hyporheic exchange can be either hydrostatic or hydrodynamic. Hydrostatic drivers are factors that increase hydraulic head, such as riverbed topography, boulders, ripples, dunes, vegetation, and channel debris. Hyporheic zones generally gain

stream water from areas with steep slopes, and flow in hyporheic zones returns to the stream when the slope is mild. Hydrodynamic drivers usually occur in high-velocity fields, and they depend on streambed permeability, bed shear stress, and roughness height (Boano et al. 2014; O'Connor et al. 2010; Stonedahl et al. 2013). Because contaminant penetrates into riverbed sediments and groundwater and returns to the stream farther downstream, the residence time in the hyporheic zone is larger than in surface storage zones, and contaminant spends more time in contact with the substrates. Therefore, representing hyporheic exchange properly is important for predicting the biogeochemistry of stream ecosystems (Bencala 2000).

To account for the effects of surface storage and hyporheic exchange separately, Choi et al. (2000) developed a two-storage-zone model that included a main channel with concentration c_m and cross-sectional area A, a surface storage zone with concentration c_s, and a subsurface zone with concentration c_h:

$$\frac{\partial c_m}{\partial t} + U\frac{\partial c_m}{\partial x} = K\frac{\partial^2 c_m}{\partial x^2} - E_s\left(c_m - c_s\right) - E_h\left(c_m - c_h\right) - \frac{q_{lat}}{A}\left(c_m - c_{lat}\right) - k_m c_m \tag{3.1}$$

$$\alpha_s\frac{\partial c_s}{\partial t} = \beta_s\left(c_m - c_s\right) - k_s c_s \tag{3.2}$$

$$\alpha_h\frac{\partial c_h}{\partial t} = \beta_h\left(c_m - c_h\right) - k_h c_h \tag{3.3}$$

Eq. (3.1) predicts the evolution of the concentration c_m in time t along the streamwise coordinate x by accounting for advection at mean velocity U, dispersion with dispersion coefficient K, exchange between the two storage zones with transfer coefficients E_s and E_h, lateral inflow with concentration c_{lat} and flow per unit length q_{lat}, and decay with rate coefficient k_m. In addition to representing exchange with the main channel, Eqs. (3.2) and (3.3) account for decay with rates k_s and k_h. The parameters α_s and α_h are the ratios of the storage zone area and main channel area for the surface storage and hyporheic zone,

respectively. The model, denoted here as TSM2, ignores any interaction between the two storage zones.

There has been a great deal of effort to identify the characteristics of contaminant transport both in the field and with lab experiments. Briggs et al. (2010) and Johnson et al. (2014) measured the area of the surface transient storage (STS) based on surveys of cross-sectional velocity. Once they located the STS, they were able to measure the concentration in the STS. The area of the hyporheic zone and concentrations in the hyporheic zone are not easy to measure using current methods. Phanikumar et al. (2007) used a wavelet decomposition method based on ADCP measurements to separate surface transient storage from hyporheic exchange by concluding that separation of the two storage mechanisms would avoid physically unrealistic solutions and parameters. Anderson and Phanikumar (2011) developed a 3D particle-transport model for the St. Clair River that compared multirate transient storages, and results indicated that TSM based on a single exchange rate is inadequate to represent complex storage dynamics in rivers.

The two-storage version of one-dimensional transport with inflow and storage (OTIS, Runkel 1998) has been widely used to simulate breakthrough curves for the main channel and two storage zones (Briggs et al. 2010; Gooseff et al. 2013; Johnson et al. 2014; Stonedahl et al. 2010). OTIS is based on the Crank-Nicholson finite difference scheme, and it allows different boundary and initial conditions to be specified. The main goal of simulation and modeling is to estimate parameters affecting transport (transfer coefficient E, fraction of the storage zone area α, inflow, etc.) for a given data set of concentration distributions. Fortunately, OTIS has a module (OTIS-P) that uses nonlinear least-squares analysis to estimate parameters involved in the contaminant transport (Runkel 1998). Wörman et al.

(2002) developed the advective storage path model (ASP model), which relates basic hydrodynamic principles of transport in rivers to streambed properties. Many studies (Briggs et al. 2010; Johnson et al. 2014; O'Connor et al. 2010; Stonedahl et al. 2013) have emphasized physical measurement of TSM parameters to decrease modeling estimation errors caused by lack of knowledge of the parameters.

Davis et al. (2000) and De Smedt et al. (2005) gave an analytical solution for the TSM with only one storage zone, whereas Kazezyilmaz-Alhan and Medina (2006) neglected surface transient storage and focused only on hyporheic zone exchange with possible advection and dispersion in the hyporheic zone. Kumar and Dalal (2014) obtained an analytical solution for a model that accounts for absorbed and dissolved solutes in the hyporheic zones. These solutions shed light on how a single storage zone can affect the contaminant transport under different circumstances. As noted by Phanikumar et al. (2007) separating surface storage from hyporheic exchange would increase realistic representation of parameters and solutions. To this end, the present study will focus on analytical solution of the two-storage model.

Methods

Dimensional analysis helps to identify the parameters that control the contaminant transport. If L is a distance downstream and a mass M of contaminant is initially injected into the main channel, then Eqs. (3.1)-(3.3) show that the main channel concentration depends on the various parameters as

$$c_m = f\left(L, t, x, U, K, E_s, E_h, \alpha_s, \alpha_h, \frac{M}{A}, \frac{q_{lat}}{A}, c_{lat}, k_m, k_s, k_h\right) \tag{3.4}$$

with similar relationships for c_s and c_h. Dimensional analysis then gives

$$C_m = \frac{c_m AL}{M} = f\left(\frac{x}{L}, \frac{Ut}{L}, \frac{K}{UL}, \frac{E_s L}{U}, \frac{E_h L}{U}, \alpha_s, \alpha_h, \frac{q_{lat} L}{AU}, \frac{c_{lat} AL}{M}, \frac{k_m L}{U}, \frac{k_s L}{U}, \frac{k_h L}{U}\right)$$
$$= f\left(X, T, \varepsilon, \beta_s, \beta_h, \alpha_s, \alpha_h, q, C_{lat}, \lambda_m, \lambda_s, \lambda_h\right) \tag{3.5}$$

The last equality defines several dimensionless parameters, including an inverse Péclet number ε, dimensionless exchange coefficients E_s and E_h, and dimensionless decay coefficients λ_m, λ_s, and λ_h. The non-dimensional governing equations are

$$\frac{\partial C_m}{\partial T} + \frac{\partial C_m}{\partial X} = \varepsilon \frac{\partial^2 C_m}{\partial X^2} - \beta_s\left(C_m - C_s\right) - \beta_h\left(C_m - C_h\right) - q\left(C_m - C_{lat}\right) - \lambda_m C_m \tag{3.6}$$

$$\alpha_s \frac{\partial C_s}{\partial T} = \beta_s\left(C_m - C_s\right) - \lambda_s C_s \tag{3.7}$$

$$\alpha_h \frac{\partial C_h}{\partial T} = \beta_h\left(C_m - C_h\right) - \lambda_h C_h \tag{3.8}$$

The initial conditions are an instantaneous slug release to the main channel and no contaminant in the two storage zones: $C_m\left(X,0\right) = \delta\left(X\right)$ and $C_s\left(X,0\right) = C_h\left(X,0\right) = 0$.

The solutions of Eqs. (3.6)-(3.8) follows the approach used by De Smedt et al. (2005) for the TSM and Schmalle and Rehmann (2014) for an advective zone model. The Laplace transform of the concentrations in zone j is given by

$$L\left[C_j\left(X,T\right)\right] = \tilde{C}_j\left(X,s\right) = \int_0^\infty e^{-sT} C_j\left(X,T\right) dT \tag{3.9}$$

The Laplace transform applied to Eqs (3.7) and (3.8) with the given initial conditions yields

$$\tilde{C}_s\left(X,s\right) = \frac{\beta_s}{\alpha_s s + \beta_s + \lambda_s} \tilde{C}_m\left(X,s\right) \tag{3.10}$$

$$\tilde{C}_h\left(X,s\right) = \frac{\beta_h}{\alpha_h s + \beta_h + \lambda_h} \tilde{C}_m\left(X,s\right) \tag{3.11}$$

which can be eliminated from the transformed version of Eq. (3.6) to obtain

$$\varepsilon \frac{\partial^2 \tilde{C}_m}{\partial X^2} - \frac{\partial \tilde{C}_m}{\partial X} - \left[s + \Gamma - \frac{\beta_s^2}{\alpha_s s + E_s + \lambda_s} - \frac{\beta_h^2}{\alpha_h s + E_h + \lambda_h} \right] \tilde{C}_m = -\delta(X) - \frac{qC_{lat}}{s} \tag{3.12}$$

where $\Gamma = \beta_s + \beta_h + q + \lambda_m$. If there is no transfer between the main channel and the two storage zones, no decay, and no lateral inflow, the solution to Eq. (3.12) is the classical ADE solution:

$$C_0(X,T) = \frac{1}{\sqrt{4\pi\varepsilon T}} \exp\left[\frac{-(X-T)^2}{4\varepsilon T} \right] \tag{3.13}$$

Therefore, the solution for Eq. (3.12) can be written as

$$\tilde{C}_m(X,s) = \tilde{C}_0\left(X, s + \Gamma - \frac{\beta_s^2}{\alpha_s s + E_s + \lambda_s} - \frac{\beta_h^2}{\alpha_h s + E_h + \lambda_h} \right) \tag{3.14}$$

To be able to invert the solution by using the generalized convolution theorem of Sneddon (1972, pp. 228-229),

$$L\left[\int_0^t F(\tau, t-\tau)\, d\tau \right] = L\left[L\left\{ L\left[F(t_1, t_2, t_3) \right] \right\} \right] \tag{3.15}$$

Eq. (3.14) is rewritten in terms of three transform variables s_1, s_2, and s_3

$$\tilde{C}_m(X, s_1, s_2, s_3) = \tilde{C}_0\left[X, (s_1 + \Gamma) - \left(\frac{\beta_s^2}{\alpha_s s_2 + \beta_s + \lambda_s} \right) - \left(\frac{\beta_h^2}{\alpha_h s_3 + \beta_h + \lambda_h} \right) \right] \tag{3.16}$$

Inverting with respect to s_1 yields

$$\tilde{C}_m(X, T_1, s_2, s_3) = C_0(X, T_1)\, \mathrm{e}^{-\Gamma T_1} \exp\left[\frac{\beta_s^2 T_1}{\alpha_s s_2 + \beta_s + \lambda_s} \right] \exp\left[\frac{\beta_h^2 T_1}{\alpha_h s_3 + \beta_h + \lambda_h} \right] \tag{3.17}$$

Then inverting with respect to s_2 and s_3, respectively, gives

$$C_m\left(X,T_1,T_2,T_3\right)= \quad C_0\left(X,T_1\right)e^{-\Gamma T_1}e^{-\Gamma_s T_2}e^{-\Gamma_h T_3}\left[\beta_s\sqrt{\frac{T_1}{\alpha_s T_2}}I_1\left(2\beta_s\sqrt{\frac{T_1T_2}{\alpha_s}}\right)+\delta\left(T_2\right)\right] \times\left[\beta_h\sqrt{\frac{T_1}{\alpha_s T_3}}I_1\left(2\beta_h\sqrt{\frac{T_1T_3}{\alpha_h}}\right)+\delta\left(T_3\right)\right] \tag{3.18}$$

where $\Gamma_s=\left(\beta_s+\lambda_s\right)/\alpha_s$, $\Gamma_h=\left(\beta_h+\lambda_h\right)/\alpha_h$, $\delta\left(z\right)$ is the Dirac delta function, and $I_1\left(z\right)$ is the Bessel function of the first kind and first order. After applying the generalized convolution theorem, the concentration in the main channel can be expressed as $C_m=C_{m1}+C_{m2}+C_{m3}+C_{m4}$, where

$$C_{m1}=C_0\left(X,T\right)e^{-\Gamma T} \tag{3.19}$$

$$C_{m2}=\beta_s\int_0^T C_0\left(X,T-\tau\right)e^{-\Gamma(T-\tau)}e^{-\Gamma_s\tau}\sqrt{\frac{T-\tau}{\alpha_s\tau}}I_1\left(2\beta_s\sqrt{\frac{\left(T-\tau\right)\tau}{\alpha_s}}\right)d\tau \tag{3.20}$$

$$C_{m3}=\beta_h\int_0^T C_0\left(X,T-\tau\right)e^{-\Gamma(T-\tau)}e^{-\Gamma_h\tau}\sqrt{\frac{T-\tau}{\alpha_h\tau}}I_1\left(2\beta_h\sqrt{\frac{\left(T-\tau\right)\tau}{\alpha_h}}\right)d\tau \tag{3.21}$$

$$C_{m4}= \quad \beta_s\beta_h\int_0^T\int_0^{T-\tau_2} C_0\left(X,T-\tau_1-\tau_2\right)e^{-\Gamma(T-\tau_1-\tau_2)}e^{-\Gamma_s\tau_1}e^{-\Gamma_h\tau_2}\frac{\left(T-\tau_1-\tau_2\right)}{\sqrt{\alpha_s\alpha_h\tau_1\tau_2}} \times I_1\left(2\beta_s\sqrt{\frac{\left(T-\tau_1-\tau_2\right)\tau_1}{\alpha_s}}\right)I_1\left(2\beta_h\sqrt{\frac{\left(T-\tau_1-\tau_2\right)\tau_2}{\alpha_h}}\right)d\tau_1 d\tau_2 \tag{3.22}$$

Although the solutions of the TSM by Davis et al. (2000) and De Smedt et al. (2005) did not provide expressions for the concentration in the storage zone, the concentrations in the surface storage and the hyporheic zones are computed here because recent studies have used grab samples or multiple probes located across the surface storage zones to report concentrations (Becker et al. 2013; Johnson et al. 2014). Eqs. (3.10) and (3.11) suggest that the concentrations C_s and C_h can be computed using either convolution or the capacitance coupling described by Young and Jones (1991):

$$C_s\left(X,T\right)=\frac{\beta_s}{\alpha_s}\int_0^T C_m\left(X,\tau\right)\exp\left[\frac{\beta_s+\lambda_s}{\alpha_s}\left(\tau-T\right)\right]d\tau \tag{3.23}$$

$$C_h\left(X,T\right)=\frac{\beta_h}{\alpha_h}\int_0^T C_m\left(X,\tau\right)\exp\left[\frac{\beta_h+\lambda_h}{\alpha_s}\left(\tau-T\right)\right]d\tau \tag{3.24}$$

Computing the concentrations in the main channel and the two storage zones requires evaluating the integrals in Eqs. (3.20)-(3.24). The adaptive Gaussian quadrature method, which requires fewer intervals than the trapezoidal rule for given accuracy, was implemented to reduce the computational cost.

Temporal moments of the concentration curves help in understanding how parameters in the governing equations affect the overall transport. Having an analytical solution for the TSM2 allows computing temporal moments from the Laplace transforms of the concentrations as described by Nordin and Troutman (1980)

$$M_n\left(X\right)=\left(-1\right)^n\left.\frac{\partial^n\tilde{C}_m}{\partial s^n}\right|_{s=0} \tag{3.25}$$

Moments are computed up to n = 4 and used to compute mean travel time of the centroid μ, variance σ^2, skewness coefficient *CSK*, and kurtosis *Kr*. They are defined in terms of the moments as

$$\begin{aligned}
\mu_m &= \frac{M_1}{M_0};\\
\sigma_m^2 &= \frac{M_2}{M_0}-\mu_m^2;\\
CSK_m &= \frac{g_m}{\sigma_m^3}=\frac{1}{\sigma_m^3}\left(\frac{M_3}{M_0}-3\mu_m\sigma_m^2-\sigma_m^3\right);\\
Kr_m &= \frac{k_m}{\sigma_m^4}=\frac{1}{\sigma_m^4}\left(\frac{M_4}{M_0}-\frac{M_3}{M_0}\mu_m+6\frac{M_2}{M_0}\mu_m^2-3\mu_m^4\right)
\end{aligned} \tag{3.26}$$

Results of these four bulk quantities for the case with no decay and lateral inflow are given in the Appendix.

Results and Discussion

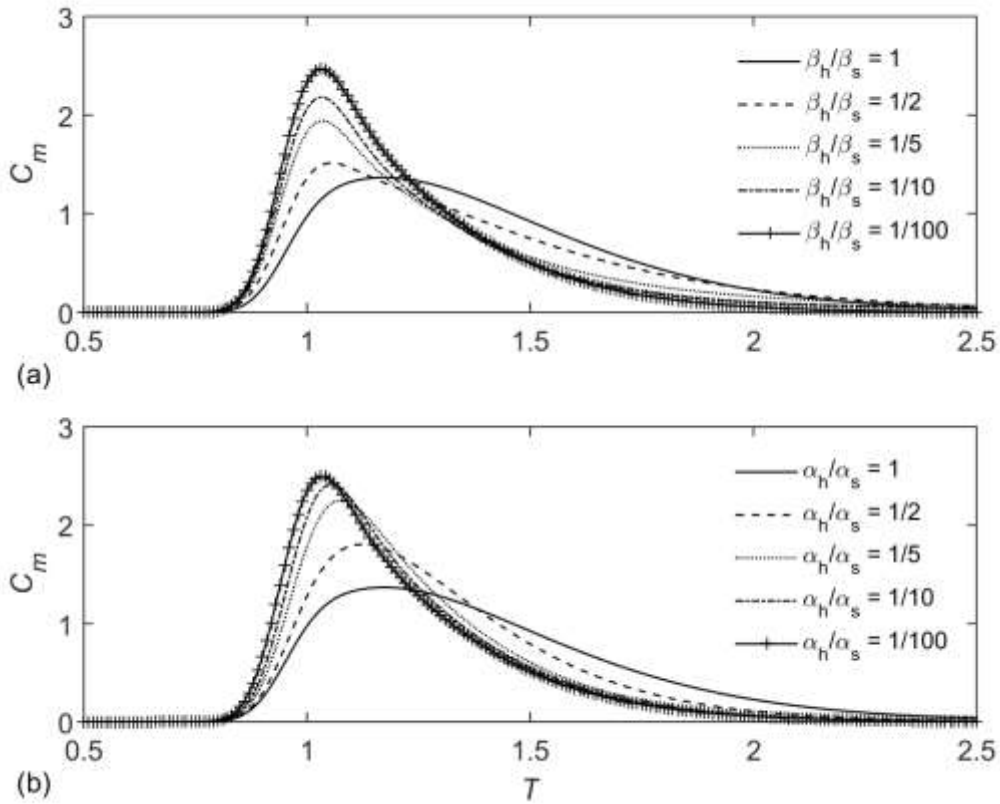

Fig. 3.1. (a) Effect of variable β_h by setting β_s constant for $\alpha_s = \alpha_h$ (b) effects of variable α_h by setting α_s constant for $\beta_h = \beta_s$ on the concentration curves with $\varepsilon = 0.0011$.

The effects of having the second (hyporheic) storage zone on the concentration curves are investigated for different ratios of the second storage zone's area and the transfer coefficient with respect to the first storage zone by setting ε constant. One of the advantages of an analytical solution is to allow the effects of parameters to be investigated easily (Fig. 3.1). The transfer coefficient and the area of the second storage zone seem to exhibit similar behavior in the concentration curves. As β_h/β_s decreases, the peak concentration in the main

channel increases due to less contaminant being transferred to the hyporheic storage [Fig. 3.1(a)]. Likewise, decreasing α_h results in increasing peak concentration because the capacity of the second storage is diminishing [Fig. 3.1(b)].

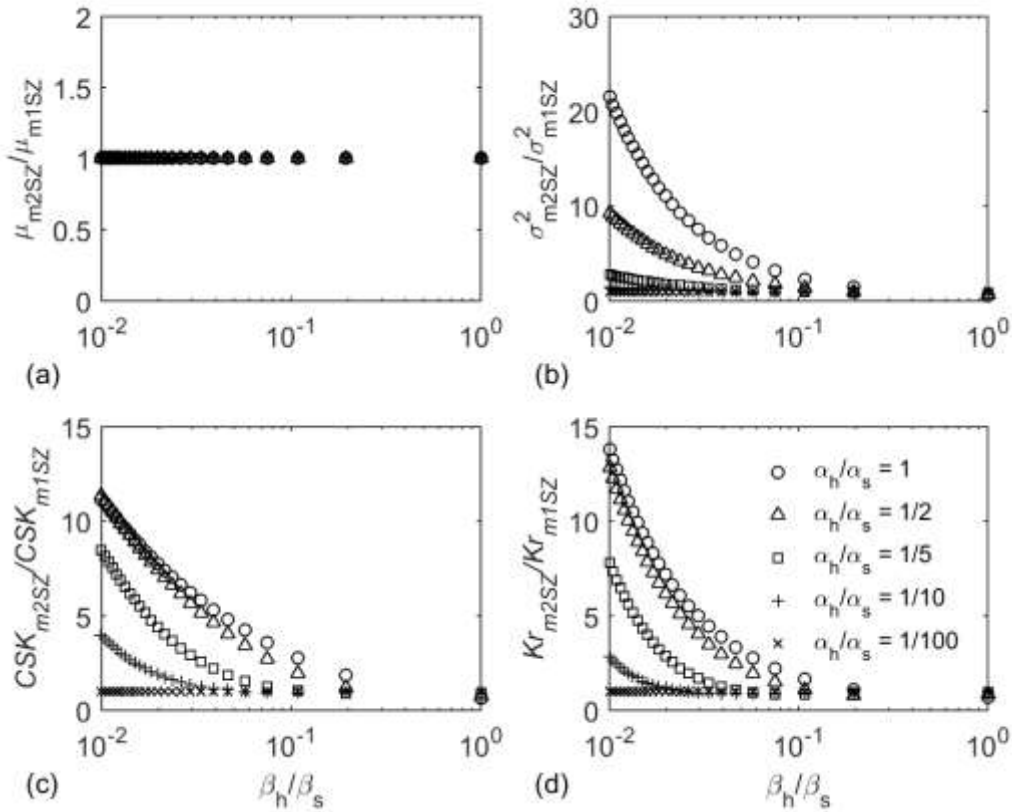

Fig. 3.2. Effects of variable α_h and β_h by setting α_s and β_s constant on (a) the arrival time of the centroid, (b) variance, (c) skewness coefficient, (d) kurtosis (ε = 0.0011 constant for all)

Although variables α_h and β_s seem to affect the spread of the data and its tail, it is not clearly seen in the concentration curves. To this end, temporal moments were computed for different ratios of the area and the transfer coefficient of the hyporheic storage with respect to surface storage parameters. The computed temporal moments for TSM2 were then normalized by the temporal moments for TSM by simply neglecting the second storage transfer coefficient and lumping together the total storage area. The arrival time of the

centroid (μ_m) is not affected by the change in the transfer coefficient (β_h) and the area of the hyporheic storage zone [Fig. 3.2(a)] because the cloud in the main channel travels at mean velocity in terms of shear dispersion and is affected only by the total storage area. If the hyporheic storage area (α_h) is less than 20% percent of the surface storage area (α_s), the variance is not affected by the hyporheic storage [Fig. 3.2 (b)]. On the other hand, smaller transfer coefficient values result in large values for skewness and the kurtosis [Fig. 3.2(c)-(d)] because a small transfer coefficient would increase the residence time of the contaminant in the hyporheic storage and cause later release, resulting in a long-tailed distribution of the concentrations.

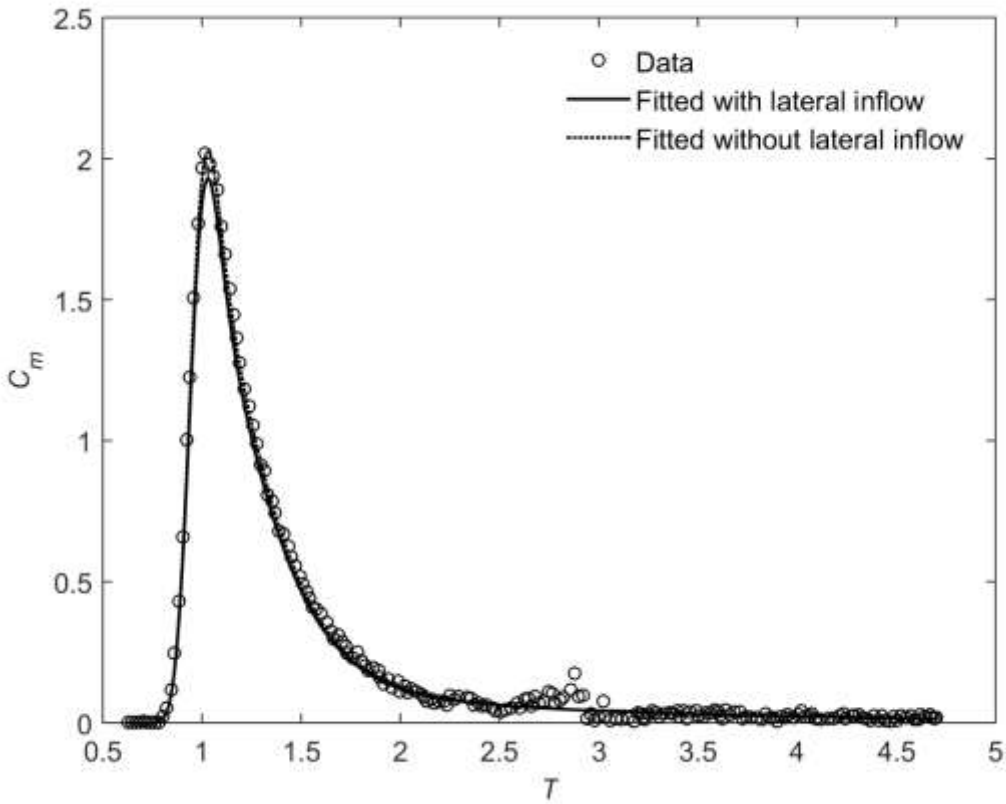

Fig. 3.3. Fitting current model to 2011 field experiment data from Johnson et al. (2014)

Johnson et al. (2014) claimed that including lateral inflow improved the fit of the model to their data. Using their parameters, the current model estimates concentrations as well as OTIS that Johnson et al. (2014) used in their fitting of the data. Although lateral inflow has little effect on the tail, it affects the peak concentration. In the 2011 experiment by Johnson et al. (2014), the peak concentration is underestimated with lateral inflow (Fig. 3.3), while the 2012 experiment including lateral inflow yields a better estimate for the peak concentration (Fig. 3.4).

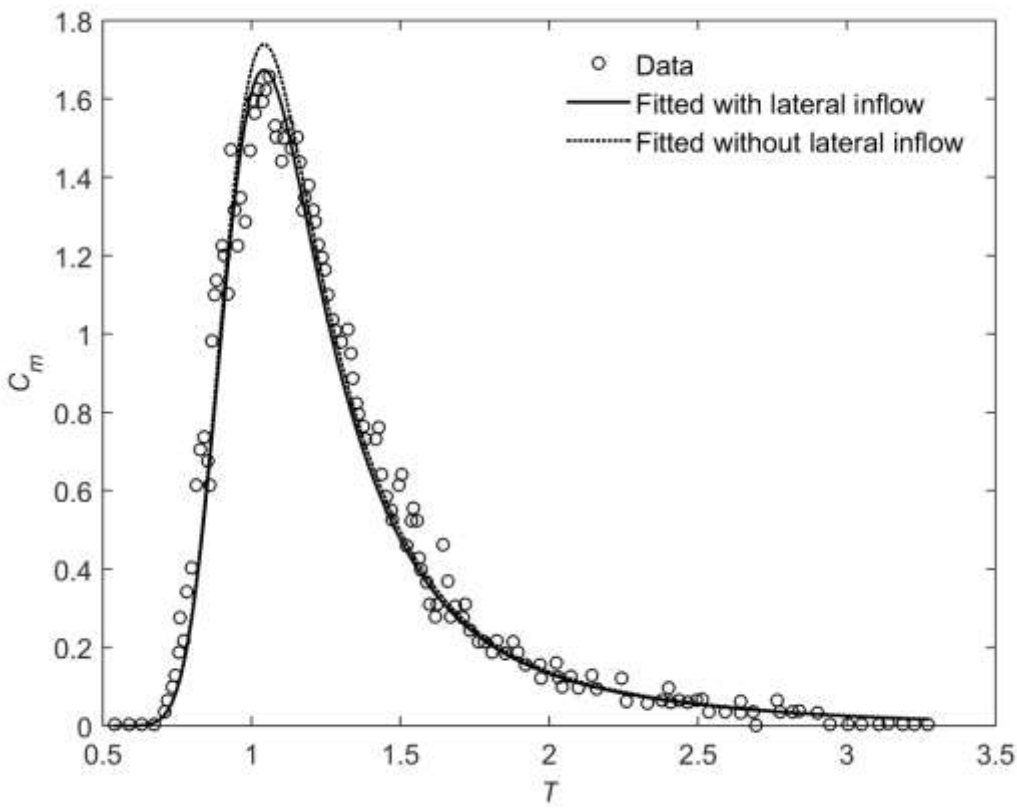

Fig. 3.4. Fitting current model to 2012 field experiment data from Johnson et al. (2014)

The analytical solution presented here complements numerical models such as OTIS. De Smedt et al. (2005) verified their analytical solution of the TSM by comparing their results to OTIS estimates for an artificial experiment. In a similar way, comparison to the

data of Johnson et al. (2014) using parameters they determined with OTIS supports the current analytical solution. The analytical solution also avoids some of the challenges of numerical modeling: Because OTIS uses a finite system and prescribed upper boundary conditions or mass flux, the parameters and the length of the reach must be calibrated to avoid the influence of the upper boundary. On the other hand, the current analytical model is obtained for an infinite system and is not affected by an upper boundary and the length of the reach. When analyzing instantaneous slug-release experiments with the TSM2, the analytical solution becomes more useful. Moreover, the standard OTIS package includes only one storage zone and must be modified to include a second storage zone. In contrast, the current model has two storage zones and can be reduced to the TSM by simply neglecting the hyporheic storage parameters in the solution.

Conclusions

The transient storage model with storage zones to account for surface storage and hyporheic storage was solved analytically using Laplace transforms and evaluated. The two storage zones interact with the main channel but not with one another. The case investigated in this study involves an initially clean river system with an instantaneous slug release into the main channel. Moreover, the analytical solution includes lateral inflow and decay parameters that can be useful for those working on nitrate removal and nutrient uptake in rivers. Although data on concentrations in the surface and hyporheic storage zones are limited, the present study illustrates how concentrations in the two storage zones can be computed if needed. Detailed analysis of the theoretical moments helps in understanding how the hyporheic storage might affect the overall transport: As the ratios of the area and the transfer coefficient for the hyporheic storage to the surface storage become smaller, hyporheic storage becomes

negligible and the model reduces to the one-storage model. Comparison with the available data in the literature shows that the solution is capable of estimating tracer response curves as well as OTIS and does not require additional effort required in applying numerical model.

References

Anderson, E. J., and Phanikumar, M. S. (2011). "Surface storage dynamics in large rivers: Comparing three-dimensional particle transport, one-dimensional fractional derivative, and multirate transient storage models." *Water Resources Research*, 47(9), 1–15.

Becker, J. F., Endreny, T. A., and Robinson, J. D. (2013). "Natural channel design impacts on reach-scale transient storage." *Ecological Engineering*, Elsevier B.V., 57, 380–392.

Bencala, K. E. (1983). "Simulation of solute transport in a mountain pool-and-riffle stream with a kinetic mass transfer model for sorption." *Water Resources Research*, 19(3), 732–738.

Bencala, K. E. (2000). "Hyporheic zone hydrological processes." *Hydrological Processes*, 14, 2797–2798.

Bencala, K. E., Gooseff, M. N., and Kimball, B. A. (2011). "Rethinking hyporheic flow and transient storage to advance understanding of stream-catchment connections." *Water Resources Research*, 47(3), 1–9.

Bencala, K. E., and Walter, R. A. (1983). "Simulation of solute transport in a mountain oil-and-riffle stream with a kinetic mass transfer model." *Water Resources Research*, 19(3), 718–724.

Boano, F., Harvey, J. W., Marion, a., Packman, a. I., Revelli, R., Ridolfi, L., and Wörman, a. (2014). "Hyporheic flow and transport processes: Mechanisms, models, and bioghemical implications." *Reviews of Geophysics*.

Briggs, M. A., Gooseff, M. N., Arp, C. D., and Baker, M. A. (2009). "A method for estimating surface transient storage parameters for streams with concurrent hyporheic storage." *Water Resources Research*, 45(4), 1–13.

Choi, J., Harvey, J. W., and Conklin, M. H. (2000). "Characterizing multiple timescales and storage zone interaction that affect solute fate and transport in drainage basin." *Water Resources Research*, 36(6), 1511–1518.

Davis, P. M., Atkinson, T. C., and Wigley, T. M. L. (2000). "Longitudinal dispersion in natural channels: 2. The roles of shear flow dispersion and dead zones in the River

Severn, U.K." *Hydrology and Earth System Sciences*., Copernicus Publications, 4(3), 355–371.

Gooseff, M. N., Briggs, M. A., Bencala, K. E., McGlynn, B. L., and Scott, D. T. (2013). "Do transient storage parameters directly scale in longer, combined stream reaches? Reach length dependence of transient storage interpretations." *Journal of Hydrology*, 483, 16–25.

Johnson, Z. C., Warwick, J. J., and Schumer, R. (2014). "Factors affecting hyporheic and surface transient storage in a western U.S. river." *Journal of Hydrology*, Elsevier B.V., 510, 325–339.

Kazezyilmaz-Alhan, C. M., and Medina, M. A. (2006). "Stream solute transport incorporating hyporheic zone processes." *Journal of Hydrology*, 329(1–2), 26–38.

Kumar, A., and Dalal, D. C. (2014). "Analytical solution and analysis for solute transport in streams with diffusive transfer in the hyporheic zone." *Journal of Hydro-Environment Research*, Elsevier B.V, 8(1), 62–73.

Nordin, C. F., and Troutman, B. M. (1980). "Longitudinal dispersion in rivers: The persistence of skewness in observed data." *Water Resources Research*, 16(1), 123–128.

O'Connor, B. L., Hondzo, M., and Harvey, J. W. (2010). "Predictive Modeling of Transient Storage and Nutrient Uptake: Implications for Stream Restoration." *Journal of Hydraulic Engineering*, 136(12), 1018–1032.

Phanikumar, M. S., Aslam, I., Shen, C., Long, D. T., and Voice, T. C. (2007). "Separating surface storage from hyporheic retention in natural streams using wavelet decomposition of acoustic Doppler current profiles." *Water Resources Research*, 43(5), 1–16.

Runkel, R. L. (1998). One-dimensional transport with inflow and storage (OTIS): a solute transport model for streams and rivers. *Water-Resources Investigations Report 98-4018*, Denver, Colorado.

Schmalle, G., and Rehmann, C. (2014). "Analytical solution of a model of contaminant transport in the advective zone of a river." *Journal of Hydraulic Engineering*, 140(7), 4014029.

De Smedt, F., Brevis, W., and Debels, P. (2005). "Analytical solution for solute transport resulting from instantaneous injection in streams with transient storage." *Journal of Hydrology*, 315(1–4), 25–39.

Sneddon, I. N. (1972). The use of integral transforms. *McGraw-Hill*, New York.

Stonedahl, S. H., Harvey, J. W., and Packman, A. I. (2013). “Interactions between hyporheic flow produced by stream meanders, bars, and dunes.” *Water Resources Research*, 49(9), 5450–5461.

Stonedahl, S. H., Harvey, J. W., Wörman, A., Salehin, M., and Packman, A. I. (2010). “A multiscale model for integrating hyporheic exchange from ripples to meanders.” *Water Resources Research*, 46(12), 1–14.

Wörman, A., Forsman, J., and Johansson, H. (1998). “Modeling retention of sorbing solutes in streams based on tracer experiment using Cr-51.” *Journal of Environmental Engineering*, 124(2), 122–130.

Wörman, A., Packman, A. I., Johansson, H., and Jonsson, K. (2002). “Effect of flow-induced exchange in hyporheic zones on longitudinal transport of solutes in streams and rivers.” *Water Resources Research*, 38(1), 2-1-2–15.

Young, W. R., and Jones, S. (1991). “Shear dispersion.” *Physics of Fluids A: Fluid Dynamics*, 3(5), 1087–1101.

Appendix. Computation of Temporal Moments

Quantities based on temporal moments for the main channel are

$$\mu_m(X) = (1+\alpha_s+\alpha_h)(X+2\varepsilon) \tag{3.27}$$

$$\sigma_m^2(X) = 2\left(\frac{\alpha_s^2}{\beta_s}+\frac{\alpha_h^2}{\beta_h}\right)(X+2\varepsilon)+2\varepsilon(1+\alpha_s+\alpha_h)^2(X+4\varepsilon) \tag{3.28}$$

$$\begin{aligned} g_m(X) = {} & 6\left(\frac{\alpha_s^3}{\beta_s^2}+\frac{\alpha_h^3}{\beta_h^2}\right)(X+2\varepsilon)+12\varepsilon(1+\alpha_s+\alpha_h)(X+4\varepsilon)\left(\frac{\alpha_s^2}{\beta_s}+\frac{\alpha_h^2}{\beta_h}\right) \\ & +4\varepsilon^2(1+\alpha_s+\alpha_h)^3(3X+16\varepsilon) \end{aligned} \tag{3.29}$$

$$\begin{aligned} k_m(X) = {} & 24\left(\frac{\alpha_s^4}{\beta_s^3}+\frac{\alpha_h^4}{\beta_h^3}\right)(X+2\varepsilon)+24\varepsilon(1+\alpha_s+\alpha_h)^2\left(X^2+12\varepsilon X+40\varepsilon^2\right)\left(\frac{\alpha_s^2}{\beta_s}+\frac{\alpha_h^2}{\beta_h}\right)+ \\ & 12\frac{\alpha_s^3}{\beta_h^2}\left\{\alpha_s X^2+\varepsilon X(4+10\alpha_s+4\alpha_h)+\varepsilon^2(16+28\alpha_s+16\alpha_h)\right\}+ \\ & 12\frac{\alpha_h^3}{\beta_h^2}\left\{\alpha_h X^2+\varepsilon X(4+4\alpha_s+10\alpha_h)+\varepsilon^2(16+16\alpha_s+28\alpha_h)\right\}+ \\ & 12\varepsilon^2(1+\alpha_s+\alpha_h)^4\left(X^2+18\varepsilon X+80\varepsilon^2\right) \end{aligned} \tag{3.30}$$

The same quantities for the surface storage zone are

$$\mu_s(x) = \frac{\alpha_s}{\beta_s}+\mu_m \tag{3.31}$$

$$\sigma_s^2(X) = \left(\frac{\alpha_s}{\beta_s}\right)^2+\sigma_m^2 \tag{3.32}$$

$$g_s(x) = 2\left(\frac{\alpha_s}{\beta_s}\right)^3+g_m \tag{3.33}$$

$$k_s = 9\left(\frac{\alpha_s}{\beta_s}\right)^4+k_m \tag{3.34}$$

These can be applied to the hyporheic storage by replacing subscript *s* with subscript *h*.

CHAPTER 4. PREDICTING TRACER RESPONSE CURVES WITH CONSTANT SKEWNESS

A paper to be submitted to the *Journal of Hydraulic Engineering*

Rusen Sinir, Chris Rehmann, and Halil Ceylan

Abstract

Estimating the arrival time and concentration of a contaminant at a water intake after a spill is crucial for planning a response to protect the public and the biota in a stream. The work in this chapter aims to provide a simple approach for predicting tracer response curves that reproduce the persistent skewness observed in field measurements. The skewness coefficient predicted by the scalene triangle method of Jobson (1997) is shown to decrease with distance from the source. A new method is developed that predicts constant skewness by describing concentration curves with the Gumbel distribution, which has a skewness coefficient of 1.1395. The two parameters affecting arrival times in the Gumbel distribution are determined with an empirical relationship between the temporal variance of the cloud and the travel time μ_t of the centroid and a regression model to predict μ_t using only discharge and distance from the source. The proposed model predicts arrival times of the leading and trailing edge better than the Jobson method, and it underestimates the peak concentration by an average of 17%. The proposed method mimics the non-Fickian behavior of the transport observed in rivers without the computational costs associated with more complex models.

Introduction

Contaminant spills in rivers threaten water supplies and the biota in affected rivers. Predicting the contaminant transport, including concentrations and arrival times at downstream sites, is important for planning responses to spills. Many models have been used

to predict contaminant concentrations (Rutherford 1994), including the one-dimensional advection-dispersion equation, the transient storage model, and the aggregated dead zone model. However, all of these methods have shortcomings, including an inability to predict the skewness observed in tracer-response curves measured in dye studies. The work in this chapter develops and evaluates an empirical model to describe observed concentration curves more reliably.

Contaminant transport is often modeled by the one-dimensional advection-dispersion equation (ADE). For example, the Incident Command Tool for Drinking Water Protection (Samuels et al. 2015), which bases its transport calculations on the ADE, was applied to predict arrival times and concentrations for a spill in the Elk River in West Virginia (Bahadur and Samuels 2015). Along with advection at the mean velocity, the ADE attributes transport to a Fickian flux proportional to a dispersion coefficient, which can be computed from empirical formulas and basic information on the flow and geometry of the channel. However, comparisons between the predictions of the ADE and results from tracer studies have demonstrated flaws in the Fickian model (e.g., Deng et al. 2004): For example, the temporal variance increases more quickly than predicted (Gonzalez-Pinzon et al. 2013), and as a result, the peak decreases more quickly than predicted (Jobson 2001). Also, while the ADE predicts that tracer response curves become symmetric far downstream of the source, measured concentration curves have long tails (Nordin and Troutman 1980). In fact, the mean value of the skewness coefficient for 384 curves was found to be approximately constant at 1.18 (Gonzalez-Pinzon et al. 2013).

Other models have tried to address the shortcomings of the ADE by accounting for trapping and release from recirculation zones. These models assume that the long tails of

tracer response curves arise from tracer entering pools, side embayments, areas with vegetation, or the subsurface and slowly returning to the main channel. For example, the transient storage model (TSM) adds exchange with a storage zone to the ADE (Bencala and Walter 1983; Nordin and Troutman 1980), and the aggregated dead zone (ADZ) model accounts for trapping through a dispersive fraction specified in each of the sub-reaches in a stream (Beer and Young 1983). Although the TSM predicts a greater magnitude of skewness than the ADE predicts, the skewness still decreases rapidly with downstream distance (Nordin and Troutman 1980). The ADZ model applied to sub-reaches in series can predict constant skewness, but specifying the number of sub-reaches is difficult because it is not a physical parameter of the system (Gonzalez-Pinzon et al. 2013).

Two other approaches for predicting contaminant transport could produce tracer response curves with persistent skewness. Jobson (1997) presented a method based on regression analysis of tracer data collected from almost 100 different rivers by the U.S. Geological Survey (USGS). Jobson (1997) represented the tracer response curve as a scalene triangle defined by the peak concentration and the arrival times of the peak and the leading and trailing edges of the contaminant cloud. To facilitate the predictions, Jobson (1997) produced empirical formulas for these parameters that require only information typically available at USGS gaging stations: the discharge at the time of interest, slope of the river, mean annual discharge, and drainage area. This method performs better than the ADE at predicting the decrease in the peak concentration with distance downstream (Jobson 1997), but its ability to predict persistent skewness has not yet been evaluated.

One functional form of the tracer response curve that does have constant skewness is the Gumbel probability distribution, which is commonly used to model extreme hydrologic

events (Brutsaert 2005). Gonzalez-Pinzon et al. (2013) noted that its skewness coefficient of 1.1395 is close to the value observed in the large dataset that they compiled, and they applied it to estimate tracer response curves by using empirical relationships based on their meta-analysis of temporal moments. However, as Gonzalez-Pinzon et al. (2013) noted, the parameters of the Gumbel distribution (and other probability distributions) have no physical connection to the tracer response curves they are used to model. Therefore, the purpose of the work in this chapter is to evaluate the skewness predicted by the Jobson method and develop an approach to predict contaminant transport with the Gumbel distribution using parameters readily available at USGS gaging stations. The next section explains the evaluation of the Jobson method and develops the new prediction method, and the following section presents the skewness predicted by the Jobson method and evaluates the new method by comparing tracer response curves in general, and arrival times and peak concentrations in particular.

Methods

Evaluating the Jobson method

The parameters of the scalene triangle used by Jobson (1997) to describe the tracer response curve depend on the arrival time of the peak concentration. As noted in the previous section, the Jobson method uses as input the discharge Q, the mean annual discharge Q_a, the drainage area D_a, and the slope S. It computes the velocity of the peak concentration using

$$V_P = 0.094 + 0.0143\left(D_a'\right)^{0.919}\left(Q_a'\right)^{-0.469} S^{0.159}\frac{Q}{D_a} \tag{4.1}$$

when the slope is known (where $Q_a' = Q/Q_a$, $D_a' = D_a^{5/4} g^{1/2}/Q_a$, and g is the acceleration of gravity) and

$$V_P = 0.02 + 0.051\left(D_a'\right)^{0.821}\left(Q_a'\right)^{-0.465}\frac{Q}{D_a} \tag{4.2}$$

when the slope is not known. The arrival time of the peak concentration at a station a distance L from the source is then computed as $t_P = L/V_P$, and the arrival time of the leading edge is $t_L = 0.89t_P$. Jobson (1997) expressed the tracer response curve in terms of a unit concentration, defined as $C_u = 10^6CQ/M$, where C is the concentration and M is the mass, and he related the unit peak concentration to its time of arrival using

$$C_{up} = 857t_P^{-0.760(Q/Q_a)^{-0.079}} \tag{4.3}$$

The time of arrival of the trailing edge, defined as the time at which the concentration falls to 10% of the peak value, is given by $t_T = t_L + t_{d10}$, where the duration is computed as $t_{d10} = 2\times10^6/C_{up}$.

The skewness coefficient predicted by the Jobson method is computed from the temporal moments. The nth moment is defined as

$$M_n = \int_0^\infty t^n C(x,t)dt \tag{4.4}$$

Then the time of arrival of the centroid μ_t, the temporal variance σ_t^2 , and the skewness coefficient γ_t are computed as

$$\mu_t = \frac{M_1}{M_0} = \frac{1}{3}\left(t_L + t_P + t_T\right) \tag{4.5}$$

$$\sigma_t^2 = \frac{M_2}{M_0} - \mu_t^2 = \frac{1}{18}\left(t_L^2 + t_P^2 + t_T^2 - t_L t_P - t_L t_T - t_P t_T\right) \tag{4.6}$$

$$\gamma_t = \frac{1}{\sigma_t^{3/2}}\left(\frac{M_3}{M_0} - 3\sigma_t^2\mu_t - \mu_t^3\right) = \frac{1}{270\sigma_t^{3/2}}\left(2t_L - t_P - t_T\right)\left(2t_P - t_L - t_T\right)\left(2t_T - t_L - t_P\right) \tag{4.7}$$

The dependence of the skewness coefficient on downstream distance is evaluated for different rivers with discharges ranging over five orders of magnitude. Data collected from USGS gaging stations for analysis of skewness are presented in Table 4.1.

Table 4.1. River discharge and drainage area data collected from USGS gaging stations.

Rivers and Gaging Stations	Q (m^3/s)	Q_a (m^3/s)	Da (km^2)
Missouri River at NE city, NE	1362.0	1130.8	1061896
Des Moines River at Fort Dodge, IA	100.8	54.2	10852
North Raccoon River near Jeferson, IA	9.7	24.7	4193
Floyed River at Alton, IA	2.3	2.7	694
Iowa River at Marshalltown, IA	17.7	27.0	3968
Sinsinawa River near Menominee, IL	0.7	0.8	103
Middle River near Indianola, IA	3.2	8.4	1268
Little Sioux River at Linn Grove, IA	29.7	22.3	4009

The proposed method

The proposed approach blends the advantages of the Jobson method and the advantages of the Gumbel probability distribution. The Gumbel distribution is given by

$$C(t) = \frac{M}{Qb}\exp\left(-\frac{(t-a)}{b}\right)\exp\left[-\exp\left(-\frac{(t-a)}{b}\right)\right] \tag{4.8}$$

where $a = \mu_t - 0.5772b$, $b = \sqrt{6\sigma_t^2 / \pi^2}$, M is the mass of contaminant injected, and Q is the discharge. In many datasets it has a constant skewness coefficient close to the value observed by Gonzalez-Pinzon, et al,. (2013), but the parameters a and b have not been related to the physical processes of contaminant transport. Following Jobson (1997), a method is developed to estimate a and b from data from USGS gaging stations. The rationale is that, in a case with negligible dispersion, the time of arrival would be $\mu_t = L/(Q/A)$, where A is the cross-sectional area of the channel. Because the geometry of the river channel is unknown in

general, an empirical relationship from Jobson (2001) can be used to estimate the cross sectional area

$$A = w_0 + w_1 Q^{w_2} \tag{4.9}$$

where w_0, w_1, and w_2 are coefficients. The second term on the right resembles the form usually used in hydraulic geometry formulas, and the first term on the right is added to account for pools and recirculation zones (Jobson 2001). Introducing an exponent θ to account for effects of dispersion yields

$$\mu_t = \frac{L^\theta}{Q}\left(w_0 + w_1 Q^{w_2}\right) \tag{4.10}$$

The four parameters θ, w_0, w_1 and w_2, were obtained by regression using data from Nordin and Sabol (1974). After estimating μ_t, σ_t^2 is estimated from the meta-analysis of Gonzalez-Pinzon et al. (2013), which yields $\sigma_t^2 = 1.629\mu_t^{1.568}$ with μ_t in s and σ_t^2 in s^2. These formulas allow a and b in the Gumbel distribution to be computed.

The proposed method was evaluated by comparing its predictions of peak concentrations and arrival times to measured values from the data compiled by Nordin and Sabol (1974) and the predictions of the ADE and the Jobson method. The arrival time of the peak is simply $t_P = a$, and the arrival times of the leading and trailing edges were defined as the times when the concentration is a fraction ϕ of the peak concentration: i.e., $C = \phi C_p$ (Fig. 4.1). These times were determined from

$$\exp\left(1 - \frac{(t-a)}{b}\right)\exp\left[-\exp\left(-\frac{(t-a)}{b}\right)\right] - \phi = 0 \tag{4.11}$$

with a root-finding algorithm. To compare with the predictions of the Jobson method, times between t_L and t_P and t_P and t_T were computed with linear interpolation. Travel times from the ADE were computed using the formulas of Rehmann (2015).

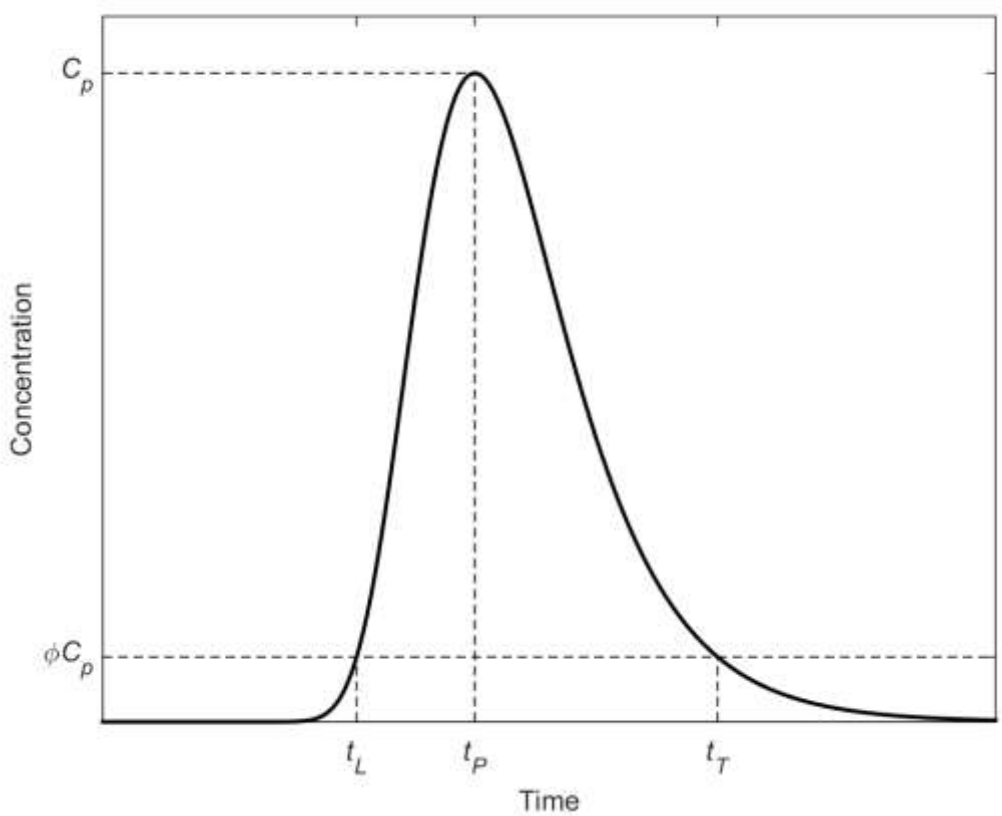

Fig. 4.1. Schematic of the peak concentration C_p and arrival times of the leading edge (t_L), peak concentration (t_P), and trailing edge (t_T). The leading and trailing edges are defined in terms of a fraction ϕ of the peak concentration.

Results and Discussion

Skewness predicted by the Jobson method

The skewness coefficient of tracer response curves predicted by the Jobson method decreases as the distance from the source increases (Fig. 4.2). This decrease occurs for rivers with discharges ranging from 0.1 m^3/s to 1000 m^3/s. The mean value of γ_t computed for these examples is 0.41, about three times smaller than the value from the meta-analysis of

Gonzalez-Pinzon et al. (2013). Like the ADE and TSM, the Jobson method does not predict persistent skewness. While the skewness from the ADE and TSM decrease as $x^{-1/2}$, the rate of decrease of skewness from the Jobson method increases as the cloud moves downstream (Fig. 4.2). This decreasing skewness suggests that the Jobson method's ability to estimate the travel time of the trailing edge will worsen downstream.

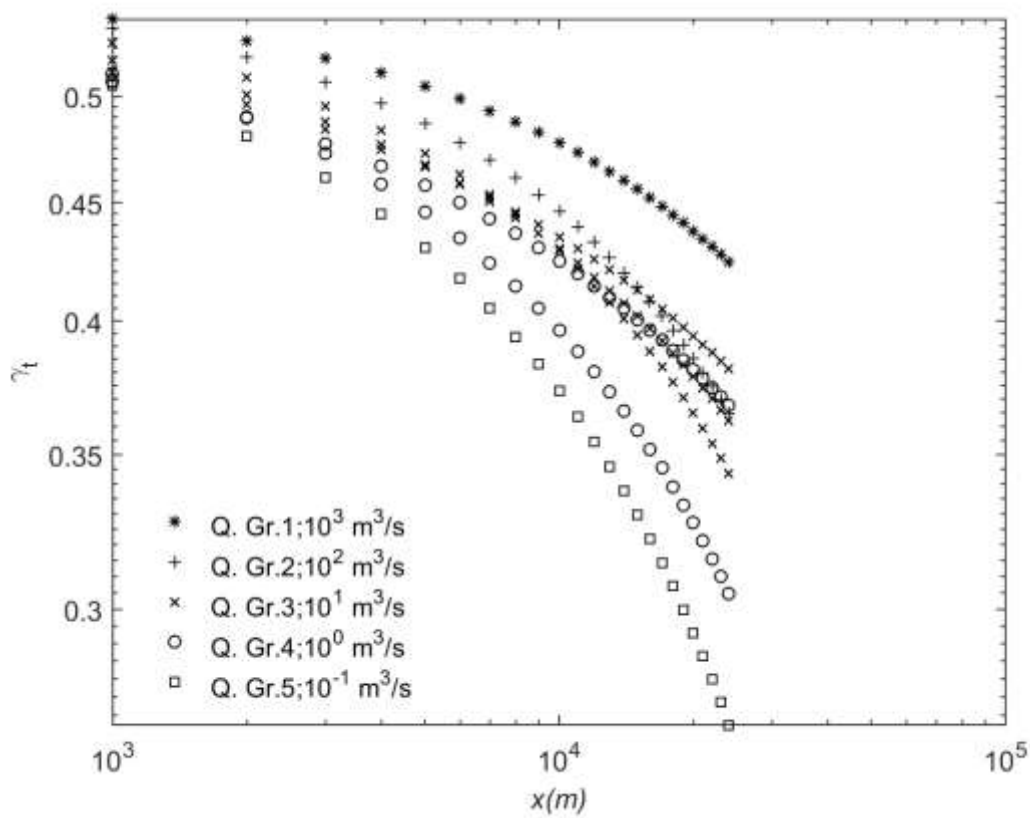

Fig. 4.2. Decrease in the skewness coefficient computed for rivers with flows ranging from 10^{-1} m^3/s to 10^3 m^3/s.

Evaluation of the proposed method

The empirical formula for the time of arrival of the centroid of the contaminant cloud [Eq. (4.10)] fits measurements well (Fig. 4.3). The regression analysis gave

$$\mu_t = \frac{L^{1.148}}{Q}\left(1.291 + 0.976Q^{0.776}\right) \tag{4.12}$$

with R^2 = 0.83. The value of the exponent θ exceeds the value of 1 that would be expected for advection only. This 15% difference reflects the faster travel of the centroid when dispersion is present. The regression compares well with the corresponding formula of Jobson (1997): Eq. (4.1) for the velocity of the peak fit measurements from a larger dataset with R^2 = 0.70. Eq. (4.12) is also simpler than the formula of Jobson (1997) because the velocity of the centroid is expressed in terms of only the distance downstream and the discharge.

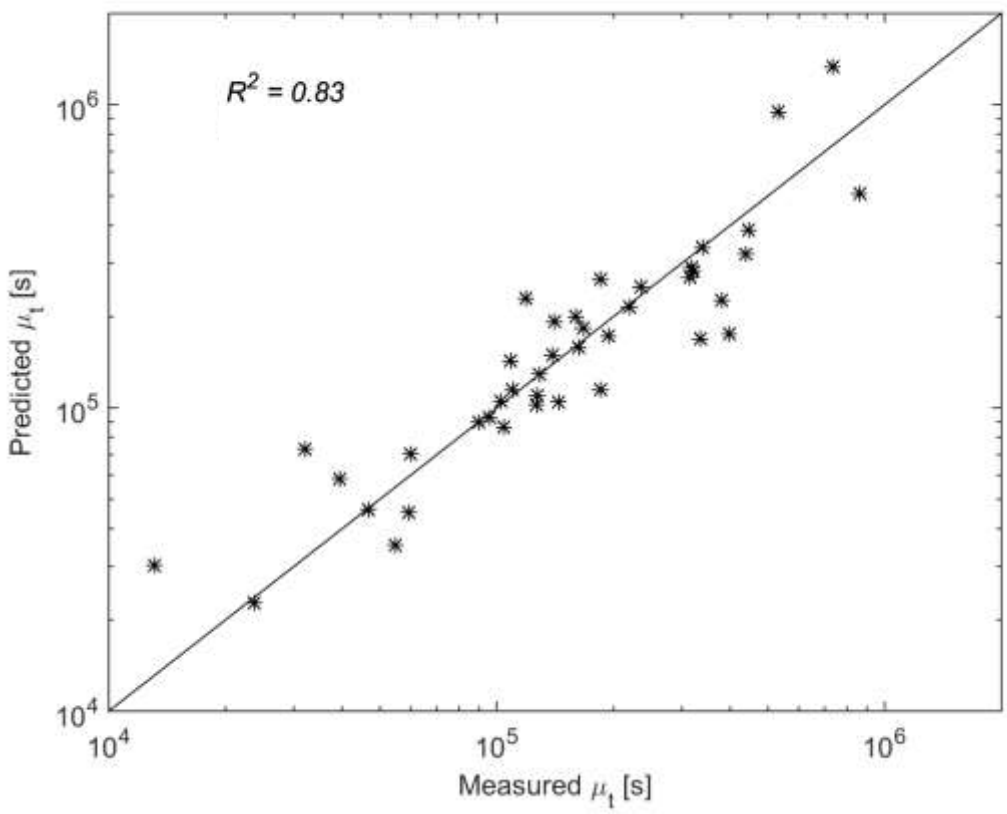

Fig. 4.3. Regression analysis to develop Eq. (4.12) for the time of arrival of the centroid

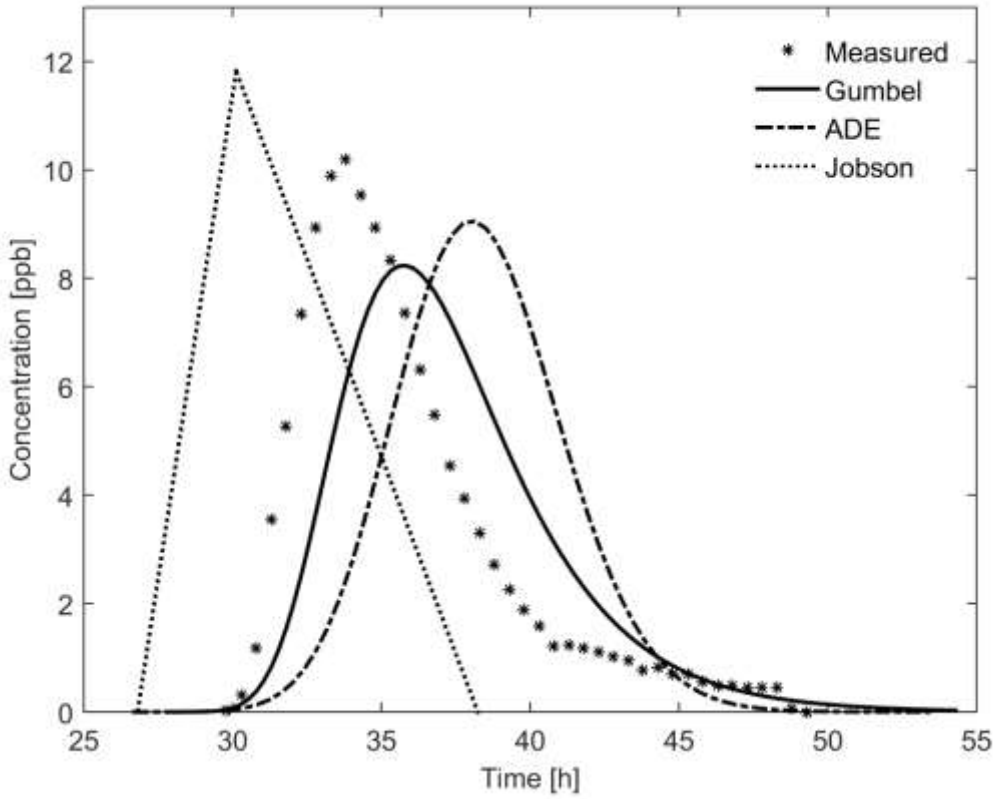

Fig. 4.4. Comparison of the tracer response curves predicted by the proposed, ADE, and Jobson methods to measured concentrations.

Comparison of the predicted tracer response curves to measured tracer response curves shows differences in the behavior of each method (Fig. 4.4). In this example, the proposed method estimates the arrival times of leading and trailing edges well, and the ADE estimates the times within about 10%. The Jobson method underestimates the arrival times, but the predictions are mostly within 10%. Both the ADE and the proposed method underestimate the peak concentration and overestimate the time of the peak, while the Jobson method overestimates the peak concentration. The proposed method better captures the long tail and skewness of the concentration curve. The Jobson method reproduces the slopes of the measured curve for times between 30 and 40 h but misses the long tail. Similarly, the curve

predicted by the ADE, which is approximately Gaussian, does not reproduce the skewness of the measurements.

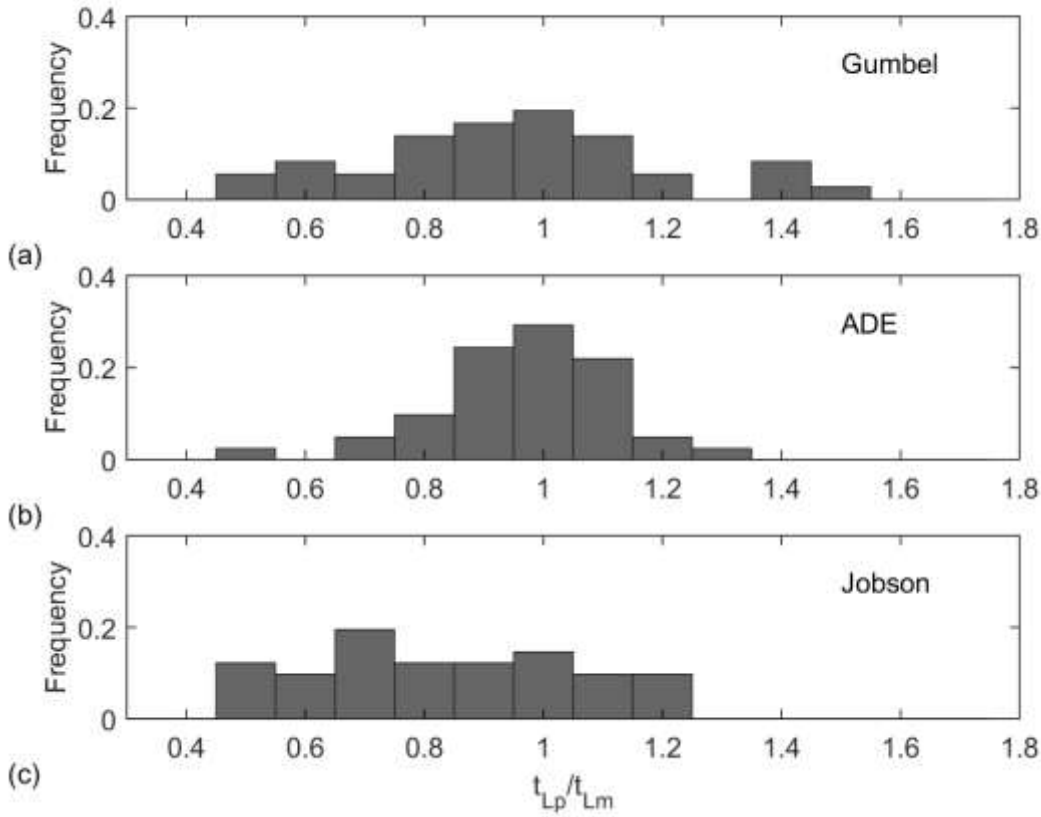

Fig. 4.5. Histograms of the ratio of the predicted and measured arrival times of the leading edge: (a) proposed method, (b) ADE method, and (c) Jobson method. The fraction ϕ is taken to be 0.1. The data for the measured times and ADE and Jobson estimates were retrieved from Rehmann (2015).

The proposed method estimates arrival times better than Jobson's method. The proposed method estimates 20% of the times of the leading edge within 95% of the measured value and 70% within 75% of the measured value [Fig. 4.5(a)]. For the same ranges, the ADE estimates 29 and 89% [Fig. 4.5(b)], and the Jobson method estimates 14 and 58% [Fig. 4.5(c)]. Similar results hold for the arrival times of the trailing edge and peak concentration. The proposed method estimates 28% of the times of the trailing edge within 95% of the

measured value and 64% within 75% of the measured value [Fig. 4.6(a)]. The ADE method estimates 34% of data within 95% and 88% within 75% [Fig. 4.6(b)], while Jobson method estimates 12 and 55% for the same range [Fig. 4.6(c)]. The proposed method estimates 14 and 67% of the arrival times of the peak within 95 and 75% of the measured values [Fig. 4.7(a)], and the Jobson method estimates 12 and 56% within the same ranges [Fig. 4.7(b)]. Although the ADE predicts arrival times better than the other methods, it requires a good estimate of the mean velocity of the river.

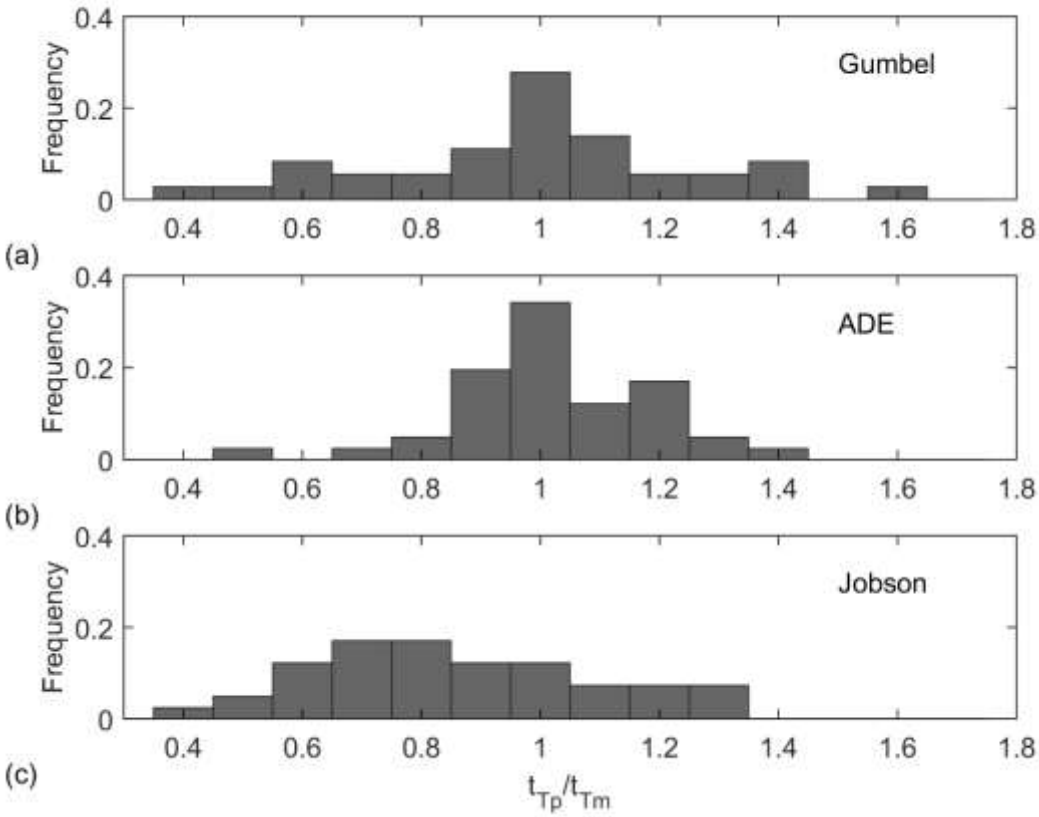

Fig. 4.6. Histograms of the ratio of the predicted and measured arrival times of the trailing edge: (a) proposed method, (b) ADE method, and (c) Jobson method. The fraction ϕ is taken to be 0.1. The data for the measured times and ADE and Jobson estimates were retrieved from Rehmann (2015).

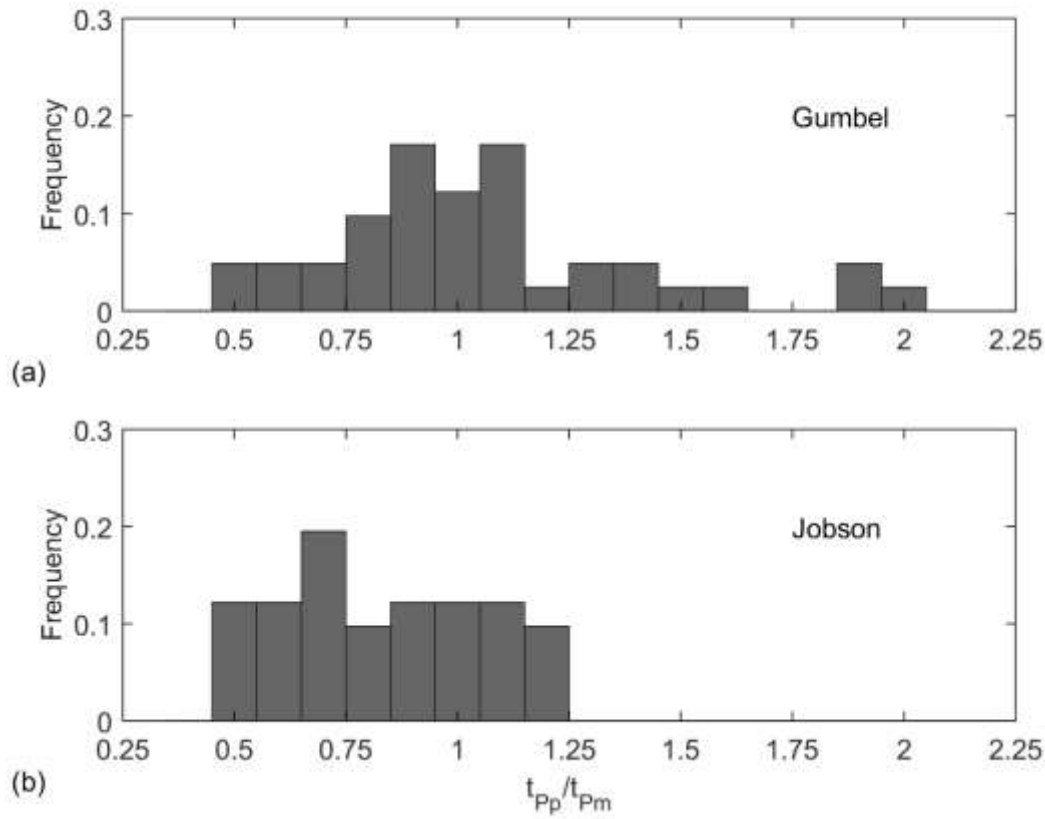

Fig. 4.7. Histograms of the ratio of the predicted and measured arrival times of the peak concentration: (a) proposed method and (b) Jobson method. The data for the measured times and Jobson estimates were retrieved from Rehmann (2015).

The ADE yields conservative estimates of the arrival times, while the proposed method and Jobson method are conservative on one side of the cloud. The Jobson method and ADE tend to underestimate the time of the leading edge, with mean ratios of predicted to measured times of 0.83 and 0.96, respectively, while the proposed method tends to overestimate with a mean ratio of 1.07. Therefore, both Jobson and ADE methods are conservative with respect to the time of first arrival of the contaminant cloud, while on average the proposed method predicts a later arrival. The Jobson method underestimates the time of the trailing edge with a mean ratio of 0.85, while the proposed method and ADE are conservative by overestimating the times with mean ratios of 1.15 and 1.02, respectively. As

discussed earlier, the Jobson method predicts decaying skewness that causes poor estimates of the trailing edge, while the proposed method predicts more accurately on the tail as expected with constant skewness.

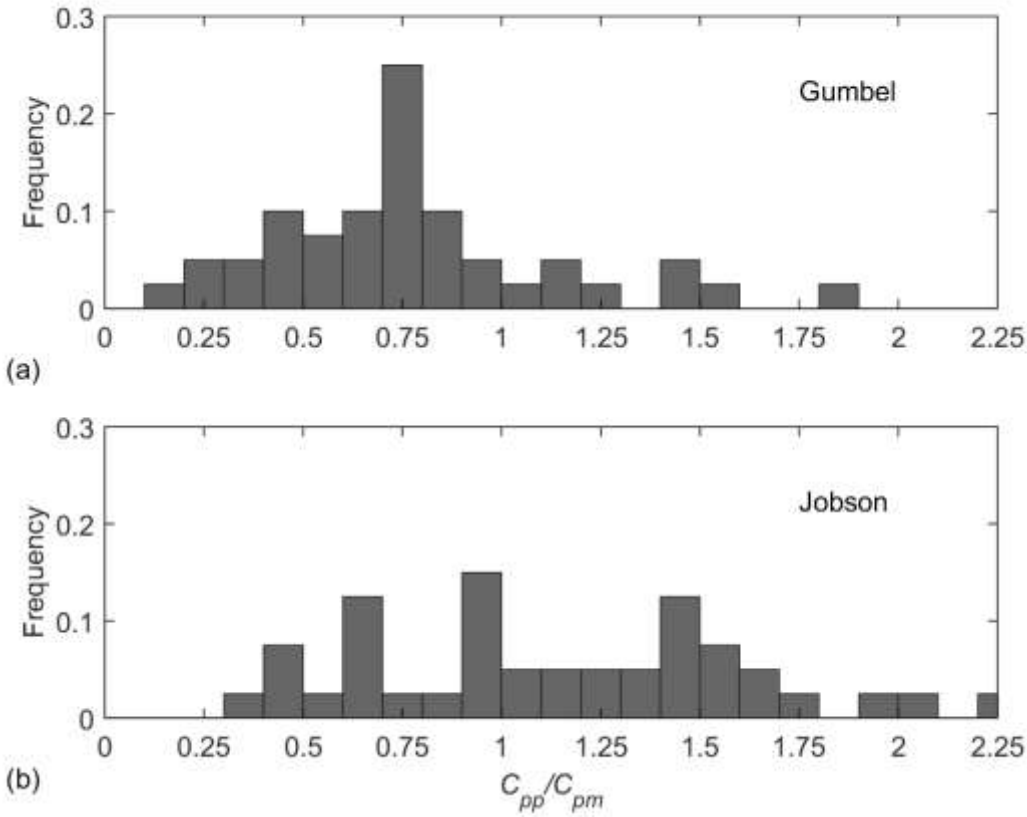

Fig. 4.8. Histograms of the ratio of the predicted to measured peak concentration: (a) proposed method and (b) Jobson method. The data for the measured times and Jobson estimates were retrieved from Rehmann (2015).

Both the proposed method and the Jobson method poorly estimate the peak concentration. The proposed method estimates 7.5% and 45% of the peak concentrations within 90% and 70% of the measured values, respectively, while the Jobson method estimates 20% and 30% for the same range. The Jobson method is conservative, with a mean ratio of the predicted to measured peak concentration of 1.18, while the proposed method tends to underestimate with a mean ratio of 0.83. In about 25% of the predictions from the

proposed method, the peak concentration is about 75% of the measured value. An overestimate of the temporal variance of the tracer response curve would lead to an underestimate of the peak concentration.

The proposed method provides a simple way to reproduce the constant skewness observed in tracer response curves. To predict concentrations downstream of a spill in a river with simple geometry, the ADE requires only the mean velocity and dispersion coefficient. However, as noted above, the skewness of the concentration curves decreases with distance from the source. The TSM requires more input and computational effort, but it fits the observed data better than the ADE. Nevertheless, it still exhibits the Fickian behavior of the ADE and suffers decaying skewness (Hunt 1999). To account for non-Fickian behavior and persistent skewness caused by longer tails, the fractional ADE has been used (Deng et al. 2004). However, few analytical solutions to the fractional ADE are available, and its numerical solution requires significant effort (Deng et al. 2004). In contrast, the proposed method reproduces tracer response curves with constant skewness using only data readily available from USGS gaging stations.

Conclusions

The work in this chapter aimed to improve predictions of arrival times and concentrations of resulting contaminant clouds so that response to spills in rivers can be improved. In particular, the proposed method presents a way to predict tracer response curves with skewness that remains constant as the cloud moves downstream. An evaluation of the behavior of the skewness coefficient γ_t predicted with the Jobson method, which models the tracer response curve as a scalene triangle, showed that, as predicted by other models, γ_t

decreases downstream. This result contrasts with measurements, which shows that γ_t is constant at approximately 1.18.

An empirical method is proposed that models the tracer response curve with the Gumbel distribution, which has a skewness coefficient (1.1395) close to the value observed in rivers. The method uses only the mass of the spilled contaminant, the discharge Q, and the distance L from the source of the spill to compute tracer response curves and estimate the arrival times of the leading edge, the trailing edge, and the peak concentration. The parameters of the Gumbel distribution are determined by regression of the arrival time of the centroid μ_t with Q and L and a relationship between μ_t and the temporal variance from Gonzalez-Pinzon et al. (2014). The proposed method predicts arrival times better than the Jobson method but underestimates the peak concentration by an average of 17%. Nevertheless, the proposed method provides a way to produce tracer response curves with constant skewness using data available at gaging stations.

References

Bahadur, R., and Samuels, W. B. (2015). "Modeling the fate and transport of a chemical spill in the Elk River, West Virginia." *Journal of Environmental Engineering*, 141(7), 5014007.

Bencala, K. E., and Walter, R. A. (1983). "Simulation of solute transport in a mountain oil-and-riffle stream with a kinetic mass transfer model." *Water Resources Research*, 19(3), 718–724.

Brutsaert, W. (2005). Hydrology: An Introduction. *Cambridge University Press*, Cambridge, U.K.

Deng, Z. Q., Singh, V. P., and Bengtsson, L. (2004). "Numerical solution of fractional advection-dispersion equation." *Journal of Hydraulic Engineering*, 130(5), 422–431.

Gonzalez-Pinzon, R., Haggerty, R., and Dentz, M. (2013). "Scaling and predicting solute transport processes in streams." *Water Resources Research*, 49(7), 4071–4088.

Hunt, B. (1999). “Dispersion model for mountain streams.” *Journal of Hydraulic Engineering*, 125(2), 99–105.

Jobson, H. E. (2001). “Predicting River Travel Time from Hydraulic Characteristics.” *Journal of Hydrologic Engineering*, 127(11), 911–918.

Nordin, C. F., and Sabol, G. F. (1974). Empirical data on longitudinal dispersion in rivers. *Water-Resources Investigations Report 20-74,* U.S Geological Survey, Washington, DC.

Nordin, C. F., and Troutman, B. M. (1980). “Longitudinal dispersion in rivers: The persistence of skewness in observed data.” *Water Resources Research*, 16(1), 123–128.

Rehmann, C. R. (2015). “Explicit Estimates of Arrival Times for Dispersion in Rivers.” *Journal of Hydraulic Engineering*, 141(11), 6015013.

Samuels, W. B., Bahadur, R., Ziemniak, C., and Amstutz, D. E. (2015). “Development and application of the incident command tool for drinking water protection.” *Water and Environment Journal*, 29(1), 1–15.

CHAPTER 5. GENERAL CONCLUSIONS

Summary

The models developed in this research are aimed at making predicting contaminant transport more effective. In Chapter 2, analytical solutions of the Reichert and Wanner (1991) model for transport near the source of a spill were obtained for different initial conditions and evaluated with the parameters estimated by Schmalle and Rehmann (2014). Chapter 3 focused on an analytical solution of a transient storage model with two storage zones that accounts for lateral inflow and decay in the main channel and the two storage zones. While the work in Chapters 2 and 3 built on the transient storage model, Chapter 4 used a different approach: The model described there represented the tracer response curve with a function that preserves the persistent skewness observed in tracer-response curves measured in field experiments.

Significant Findings

- The analytical solutions of the advective zone model in Chapter 2, which apply to a contaminant spill in the stagnant zone of a river and maintained pollution in the flowing zone, expand the information available for constructing solutions for more complex mixing situations in the advective zone of a river.
- Compared to the case of a flowing zone spill, contaminant clouds for a stagnant zone spill travel more slowly, spread more, and shift from positive to negative skewness. These differences are due to an initial delay in advection of the cloud caused by the transfer from the stagnant zone to the flowing zone.
- The solution for a maintained injection in the flowing zone differs from that produced using the ADE only at small times and distances from the source.

- The analytical solution of the transient storage model with two storage zones gives an efficient way of estimating downstream concentrations of an instantaneous slug release with lateral inflow and decay. The analytical solution avoids the need to define upper boundary conditions and account for finite reach length that constrains numerical models.
- Even if the transfer coefficient of the subsurface storage zone is small compared to the transfer coefficient of the surface storage zone, subsurface storage still affects the tracer response curves and the bulk quantities of the curves.
- The Jobson method predicts decaying skewness, as do the ADE and TSM. Therefore, the Jobson method cannot reproduce observed persistent skewness from tracer response curves in field measurements.
- The empirical model with constant skewness predicts travel times better with fewer parameters than required by Jobson's method.

Future Work

Further research related to the work in Chapter 2 would be exploring and evaluating new cases of contaminant transport near the source, and building a code package that could be utilized for different scenarios using superposition methods.

Estimating many of the parameters involved in Chapter 3 with measurements and relating them to flow conditions would reduce the need for tracer studies. An example of such a task would be using an acoustic Doppler current profiler to predict the transfer coefficient between the main channel of a river and the recirculation zones to separate the area of the recirculation zones from the main channel. Having more measured parameters would not only provide more realistic results but also allow for more practical parameter estimation from temporal moments of the tracer response curves.

Defining a scaling factor for mean arrival time with respect to discharge and distance from source would increase the accuracy of the estimations described in Chapter 4. Defining new empirical relationships for rivers that have similar magnitudes of discharge would also increase the accuracy.